

Interdecadal Connection between Arctic Temperature and Summer Precipitation over the Yangtze River Valley in the CMIP5 Historical Simulations

YUEFENG LI

Pacific Northwest National Laboratory, Richland, Washington, and China Meteorological Administration Training Center, WMO Regional Training Center, Beijing, China

L. RUBY LEUNG

Pacific Northwest National Laboratory, Richland, Washington

ZINIU XIAO

China Meteorological Administration Training Center, WMO Regional Training Center, Beijing, China

MIN WEI

National Meteorological Information Center, Beijing, China

QINGQUAN LI

National Climate Center, Beijing, China

(Manuscript received 6 November 2012, in final form 22 March 2013)

ABSTRACT

This study assesses the ability of the Coupled Model Intercomparison Project phase 5 (CMIP5) simulations in capturing the interdecadal precipitation enhancement over the Yangtze River valley (YRV) and investigates the contributions of Arctic temperature and mid- to high-latitude warming to the interdecadal variability of the East Asian summer monsoon rainfall. Six CMIP5 historical simulations including models from the Canadian Centre for Climate Modeling and Analysis (CCCma), the Beijing Climate Center, the Max Planck Institute for Meteorology, the Meteorological Research Institute, the Met Office Hadley Centre, and NCAR are used. The NCEP–NCAR reanalysis and observed precipitation are also used for comparison. Among the six CMIP5 simulations, only CCCma can approximately simulate the enhancement of interdecadal summer precipitation over the YRV in 1990–2005 relative to 1960–75; the various relationships between the summer precipitation and surface temperature (T_s), 850-hPa winds, and 500-hPa height field (H500); and the relationships between T_s and H500 determined using regression, correlation, and singular value decomposition (SVD) analyses. It is found that CCCma can reasonably simulate the interdecadal surface warming over the boreal mid- to high latitudes in winter, spring, and summer. The summer Baikal blocking anomaly is postulated to be the bridge that links the winter and spring surface warming over the mid- to high latitude and Arctic with the enhancement of summer precipitation over the YRV. Models that missed some or all of these relationships found in CCCma and the reanalysis failed to simulate the interdecadal enhancement of precipitation over the YRV. This points to the importance of Arctic and mid- to high-latitude processes on the interdecadal variability of the East Asian summer monsoon and the challenge for global climate models to correctly simulate the linkages.

1. Introduction

As has been well documented, the East Asian summer monsoon circulation has become weaker after an abrupt climate shift near the end of the 1970s (Chen and Wu

Corresponding author address: Dr. L. Ruby Leung, Atmospheric Sciences and Global Change Division, Pacific Northwest National Laboratory, 902 Battelle Blvd., Richland, WA 99352.
E-mail: ruby.leung@pnl.gov

2000; Lau and Weng 2001; Wang 2001; Ding et al. 2008; Zhou et al. 2009a; Wang et al. 2010). Consistent with the circulation change, there has been an overall increase of precipitation intensity in southern China since the late 1970s, which peaked in the middle of the 1990s (Zhao et al. 2010; Lei et al. 2011), and a corresponding drying trend in north China (Chen et al. 2006). Previous studies have demonstrated the impacts of surface climate conditions [e.g., sea surface temperature (SST)], Tibetan Plateau (TP) snow cover and heating, and anomalous circulation at the lower midlatitudes on interdecadal variations of the East Asian summer monsoon using observations, reanalyses, and numerical experiments.

As land–sea thermal contrast is a primary force of the monsoon system, surface temperatures (T_s) have important impacts on the monsoon circulation and precipitation. Improved simulations of T_s in the Community Climate System Model, version 4 (CCSM4; compared to CCSM3), as a result of improved simulation of El Niño–Southern Oscillation (ENSO) have been shown to improve many aspects of the Asian–Australian monsoon simulations (Meehl et al. 2012). Despite the importance of T_s , Wang et al. (2011) analyzed 26 simulations from 11 GCMs of the Atmospheric Model Intercomparison Project II (AMIP II) and revealed a basic inability of the models to simultaneously predict the Yangtze River valley (YRV) precipitation annual cycle and summer interannual variability in response to observed global SST distributions. Zhou et al. (2009b) demonstrated that the East Asian summer monsoon has the lowest reproducibility among the Asian–Australian monsoon subsystems in a multimodel set of atmospheric simulations forced by historical SSTs and greenhouse gases and aerosol forcing agents for the period of 1950–99. They attributed the model failure to specifying the correct historical SST to capture the change in zonal land–sea thermal contrast across East Asia.

Wu et al. (2012) established the role of the TP snow cover in modulating the ENSO teleconnections, which in turn, modulates the ENSO–East Asian summer monsoon relationship as the Rossby wave response to the ENSO diabatic forcing is enhanced when the TP snow cover is reduced in the summer. This is consistent with the fact that the diabatic forcing associated with anomalies of the TP snow cover is an important forcing of large-scale atmospheric circulation that can exert profound influences on climate variability downstream (e.g., Wang et al. 2008; Lin and Wu 2011; Wu et al. 2012). In contrast to ongoing climate warming, a weakening trend in sensible heating has been persistent over most of the TP. The weakening trend in sensible heating over the TP is primarily a response to the spatial nonuniformity of large-scale warming over the East Asian continent, which is

characterized by much greater warming at mid- to high latitudes than over the tropics and subtropics. However, no significant stable correlation exists between the TP sensible heating source and the overall trend or interdecadal variability in the East Asian summer monsoon (Duan et al. 2011).

In addition to T_s and TP snow cover, the summer precipitation reduction in north China has a good correlation with the Northern Hemispheric circulation changes (Hao et al. 2010). Yu et al. (2004) found a distinctive strong tropospheric cooling trend in East Asia during July and August. The cooling trend is most prominent at the upper troposphere around 300 hPa. Accompanying this summer cooling, the upper-level westerly jet stream over East Asia shifts southward and the East Asian summer monsoon weakens, which results in the tendency toward increased droughts in northern China and floods in the YRV. These observational evidences raise the possibility that the East Asian summer tropospheric cooling may be linked to the stratosphere temperature changes.

Lastly, Arai and Kimoto (2005) found that when T_s over Siberia is high in April, blocking events occur more frequently than normal over northeastern Siberia and the Okhotsk Sea in May and June. Associated with the enhanced blocking activity, the surface Okhotsk high intensifies in May and June, affecting the East Asia early summer precipitation (Wang et al. 2009). Li and Ding (2004) found the interannual and interdecadal features for the blockings over the mid- to high latitudes of Eurasia. Also, the first leading mode of precipitation over eastern China during the mei-yu season (June and July) shows a precipitation oscillation between the YRV and south China, which has clear interannual and interdecadal variations and is associated with an interdecadal component of positive geopotential height anomaly over Eurasia and a positive anomaly of the subtropical high over East Asia (Ma et al. 2012).

So far our discussion indicates the impacts of temperature and height conditions, particularly over the tropics and the low to middle latitudes, on the Asian summer monsoon. However, some studies have investigated the impact of processes in the mid- to high latitudes on Asian summer monsoon. For example, Wang and Zhang (2010) selected four coupled climate models used in the third phase of the Coupled Model Intercomparison Project (CMIP3) to project the summer climate conditions over East Asia once the Arctic becomes ice-free beginning in the 2060s. Their results show that the East Asian summer monsoons will tend to be stronger and that the water vapor transport to central northern China will be strengthened, leading to increased summer precipitation in central northern China and overall increase in precipitation in

northwest China under ice-free Arctic summer conditions. Li and Leung (2013) noted the increase in T_s over the Arctic since the late 1970s. They showed, using regression of the Arctic spring and summer temperature onto the time coefficients of the leading interannual and interdecadal precipitation modes, that interdecadal summer precipitation in China is related to the Arctic spring warming. However, the contributions of warming over the mid- to high latitudes and the Arctic and the variations of height fields to the summer precipitation over the YRV are generally less well understood compared to the other factors discussed above.

Simulating the Asian summer monsoon and the associated precipitation remains a significant challenge in climate modeling. Given the prominent and well-documented decadal trends in the East Asian monsoon and precipitation discussed above, this study aims to assess the ability of the historical simulations in the fifth phase of the Coupled Model Intercomparison Project (CMIP5) to capture the decadal features and to investigate the contributions of mid- to high-latitude and Arctic warming to the interdecadal variability of the summer monsoon precipitation over the YRV. Such investigations may provide further insights on possible mechanisms that play important roles in the interdecadal variation of summer precipitation over the YRV.

In what follows, section 2 describes the six models and data used in our analyses. Characteristics of the interdecadal variations of summer precipitation over China and T_s of the (preceding) winter, spring, and summer are shown in section 3. In section 4, interdecadal regressions of the winter, spring, and summer T_s on the summer precipitation variation over the YRV are performed. In section 5, relationships between the summer precipitation over the YRV and atmospheric circulations are investigated. In section 6, relationships between T_s over the boreal mid- to high latitudes and the Arctic and the 50-hPa height fields (H500) in the winter, spring, and summer are explored using singular value decomposition (SVD) analysis. In section 7, mechanisms of how the boreal mid- to high-latitude T_s influences summer precipitation over the YRV are discussed. Finally, the conclusion and discussion are presented in section 8.

2. Models and data

CMIP5 includes a comprehensive suite of modeling experiments performed using coupled atmosphere-ocean global climate models and some simulations included carbon cycles (Taylor et al. 2012). One set of experiments simulates the past climate using historical forcings (e.g., greenhouse gases, aerosols, land use, and volcanic activities) from 1850 to 2005 to evaluate how

realistic the models can simulate trends and variability of the observational records. We select simulations produced by six countries including Canada, China, Germany, Japan, the United Kingdom, and the United States. Although six models is a relatively small sample, they represent a good range of diversity based on the GCM genealogy of Masson and Knutti (2011) and model resolution. Monthly model outputs used in our analysis include precipitation rate, T_s , winds (u , v , and ω), and geopotential height (http://cmip-pcmdi.llnl.gov/cmip5/data_portal.html). Descriptions of the models can be found in Table 1. Hereafter, we use abbreviations to discuss simulations from the various models: Beijing Climate Center (BCC) of China, Meteorological Research Institute (MRI) of Japan, Met Office Hadley Centre (MOHC) of the United Kingdom; Max Planck Institute for Meteorology (MPI-M) of Germany, Canadian Centre for Climate Modeling and Analysis (CCCma) of Canada, and National Center for Atmospheric Research (NCAR) of the United States.

Observed monthly precipitation is derived from the National Meteorological Information Center in China, which includes observations from 743 stations. However, only 350 stations with continuous observations from 1956 to 2005 are used in this study. We also use data from the NCEP-NCAR Reanalysis 1 project (Kalnay et al. 1996), which used a state-of-the-art analysis/forecast system with data assimilation to provide analysis of the atmospheric states from 1948 to the present. Variables are classified into four categories from A to D, depending on the degree to which they are influenced by the observations (class A) and/or the model (class D): T_s (class B), wind (u and v , class A; ω , class B), geopotential height (class A), and precipitation rate (class C) are used. The NCEP-NCAR reanalysis data are provided by the National Oceanic and Atmospheric Administration (NOAA)/Oceanic and Atmospheric Research (OAR)/Earth System Research Laboratory (ESRL) Physical Sciences Division (PSD) from their website (<http://www.esrl.noaa.gov/psd/>).

This study focuses on analysis of data on the mainland of eastern China. We define south China at 100°–120°E, 22°–27°N; the YRV at 100°–120°E, 27°–33°N; and north China at 100°–120°E, 33°–42°N, based on the distribution of observed climatological precipitation in Fig. 1h. Regression and correlation analyses are carried out for the six model simulations and the NCEP-NCAR reanalysis data during 1956–2005, and statistical significances reaching and exceeding the 95% confidence levels are noted. The threshold is reduced to 90% for summer precipitation because precipitation of the East Asian summer monsoon has very large interannual variability and because model skill in reproducing the observed precipitation is generally low. Comparisons of interdecadal

TABLE 1. The six CMIP5 model simulations used in the present study. Detailed descriptions of the models and the data are available online at <http://cmip-pcmdi.llnl.gov/cmip5/>.

Institution	Model	Atmosphere model and resolution	Horizontal and vertical resolution of output data
Beijing Climate Center (BCC), China	Beijing Climate Center, Climate System Model, version 1.1 (BCC_CSM1.1)	BCC, Global Atmospheric Climate Model, version 2.1 (BCC_AGCM2.1) T42L26	$128 \times 64 \times 17$
Meteorological Research Institute (MRI), Japan	Meteorological Research Institute Coupled Atmosphere–Ocean General Circulation Model, version 3 (MRI-CGCM3)	Global Spectral Model (GSMUV) TL159L48	$320 \times 160 \times 23$
Met Office Hadley Centre (MOHC), United Kingdom	Hadley Centre Coupled Model, version 3 (HadCM3)	Hadley Centre Atmospheric Model, version 3 (HadAM3) N48L19	$96 \times 72 \times 17$
Max Planck Institute for Meteorology (MPI-M), Germany	Max Planck Institute Earth System Model, low resolution (MPI-ESM-LR)	ECHAM6 T63L47	$192 \times 96 \times 25$
Canadian Centre for Climate Modeling and Analysis (CCCma), Canada	Second Generation Canadian Earth System Model (CanESM2)	Canadian Atmospheric Model, version 4 (CanAM4) T63L35	$128 \times 64 \times 22$
National Center for Atmospheric Research (NCAR), United States	Community Climate System Model, version 4 (CCSM4)	Community Atmosphere Model 4 (CAM4) $288 \times 200 \times 26$	$288 \times 192 \times 17$

variations are performed between 1990 and 2005 (after the climate shift) and 1960 and 1975 (before the climate shift) using composite maps of the difference between the averages for 1990–2005 and 1960–75 for precipitation, temperature, and atmospheric circulation. The confidence levels of the composite pattern are produced using the Student's *t* test. Characteristics of the composite patterns for precipitation, temperature, and circulation will be noted when the statistical significance is equal to or exceeds the 95% confidence level.

3. Interdecadal variations between 1990–2005 and 1960–75

a. Summer precipitation over China

The summer precipitation over China is a key indicator of monsoon intensity and an important performance metric to evaluate models' ability to simulate the Asian summer monsoon. The dominant pattern of summer averaged precipitation (climatological pattern) over China from 1956 to 2005 is reproduced by most models (Fig. 1). However, the simulated precipitation is more prominent over the southern and southeastern TP in BCC, MRI, MPI-M, CCCma, and NCAR (Figs. 1a,b,d,e,f) than the observations (Fig. 1h). The positive bias may be related to the amplified terrain forcing and/or the stronger-than-observed southwestern monsoonal air flows from Somali toward the TP. Only MOHC did not produce a marked increase in precipitation over the southern and

southeastern TP (cf. Fig. 1c with Fig. 1h), but the simulated precipitation is still more than observed. MRI (Fig. 1b) reduces excessively the precipitation from south China toward the YRV and north China relative to the observed climatology (Fig. 1h). The NCEP Climate Forecast System also exaggerates the precipitation over the southern–southeastern hills of the TP (Gao et al. 2011). There is not a clear difference in the simulated precipitation climatology separating models with lower versus higher horizontal resolution.

As discussed earlier, precipitation over eastern China has gone through a significant decadal adjustment, with most of north and northeast China suffering from severe and persistent droughts while the YRV and south China have experienced more heavy rainfall and flood events, since the end of the 1970s (Hu 1997; Weng et al. 1999; Chen and Wu 2000; Lau and Weng 2001; Wang 2001; Hu et al. 2003; Yang and Lau 2004; Zhang et al. 2004; Ho et al. 2005; Chen et al. 2006; Ding et al. 2008, 2009). These interdecadal variations of observed precipitation are shown clearly in Fig. 2h, with obvious increases over the YRV in 1990–2005 compared to 1960–75. The shadings denote the significance of the composite pattern exceeding the 90% (green) and 95% (blue) confidence level by the Student's *t* test. Only CCCma can approximately simulate the enhancement of interdecadal precipitation (Fig. 2e). MRI and MPI-M (Figs. 2b,d) can simulate the enhanced precipitation over small areas of the YRV. The interdecadal variations of precipitation simulated by MOHC (Fig. 2c, low horizontal resolution)

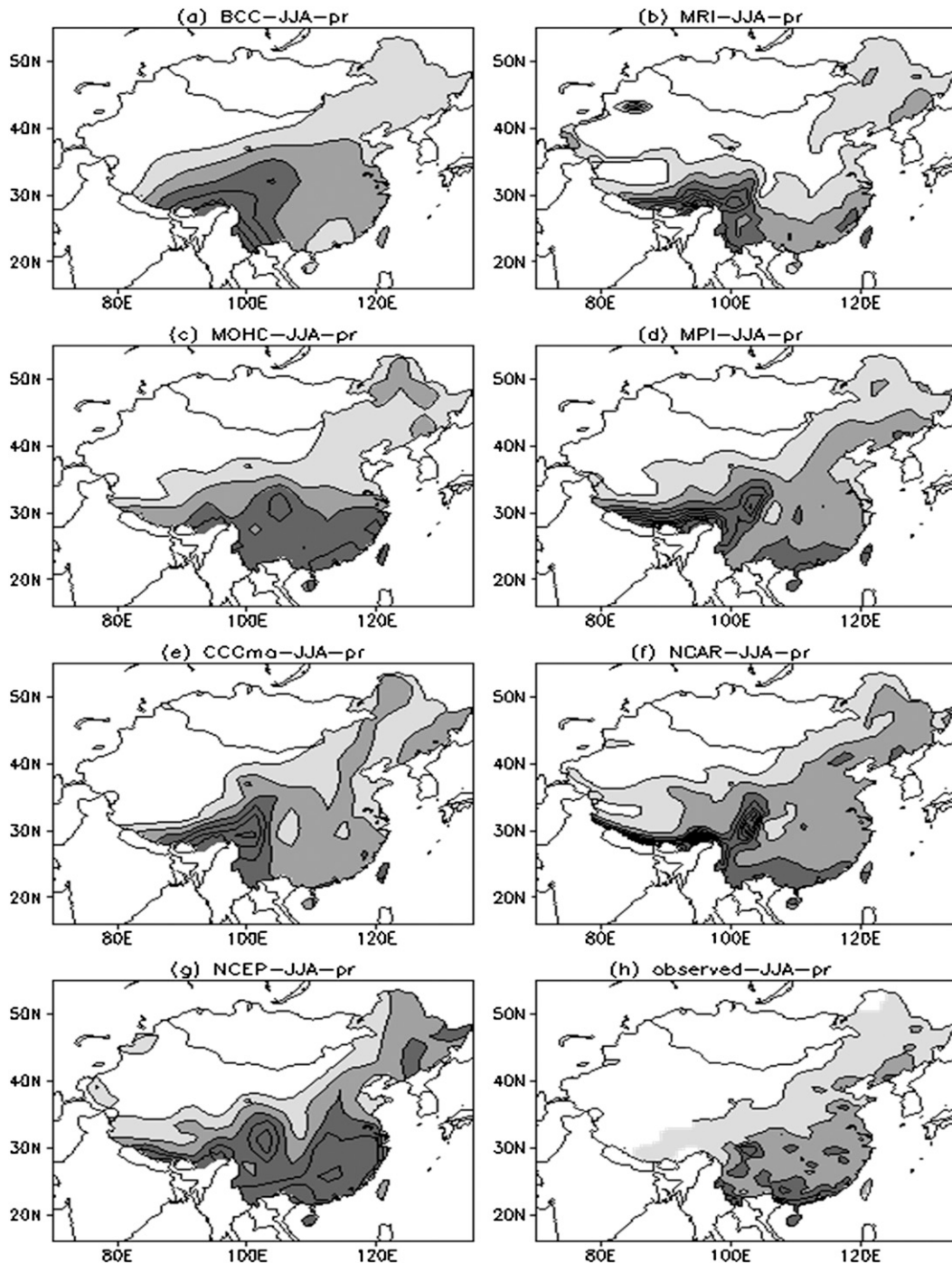


FIG. 1. The summer averaged precipitation over China from 1956 to 2005 for (a) BCC, (b) MRI, (c) MOHC, (d) MPI-M, (e) CCCma, (f) NCAR, (g) the NCEP-NCAR reanalysis, and (h) observations. The contour interval is $200 \text{ kg m}^{-2} \text{ summer}^{-1}$. The light, middle, and dark shaded areas denote precipitation larger than 200, 400, and $600 \text{ kg m}^{-2} \text{ summer}^{-1}$, respectively.

and NCAR (Fig. 2f, high horizontal resolution) are completely opposite to the observations over the YRV, although their horizontal resolutions are very different (Table 1). The NCEP-NCAR reanalysis shows larger

variation amplitude of the interdecadal precipitation (Fig. 2g), but the variation pattern is basically correct (wet in the south and dry in the north) over eastern China, even though precipitation is class C data (Kalnay et al. 1996).

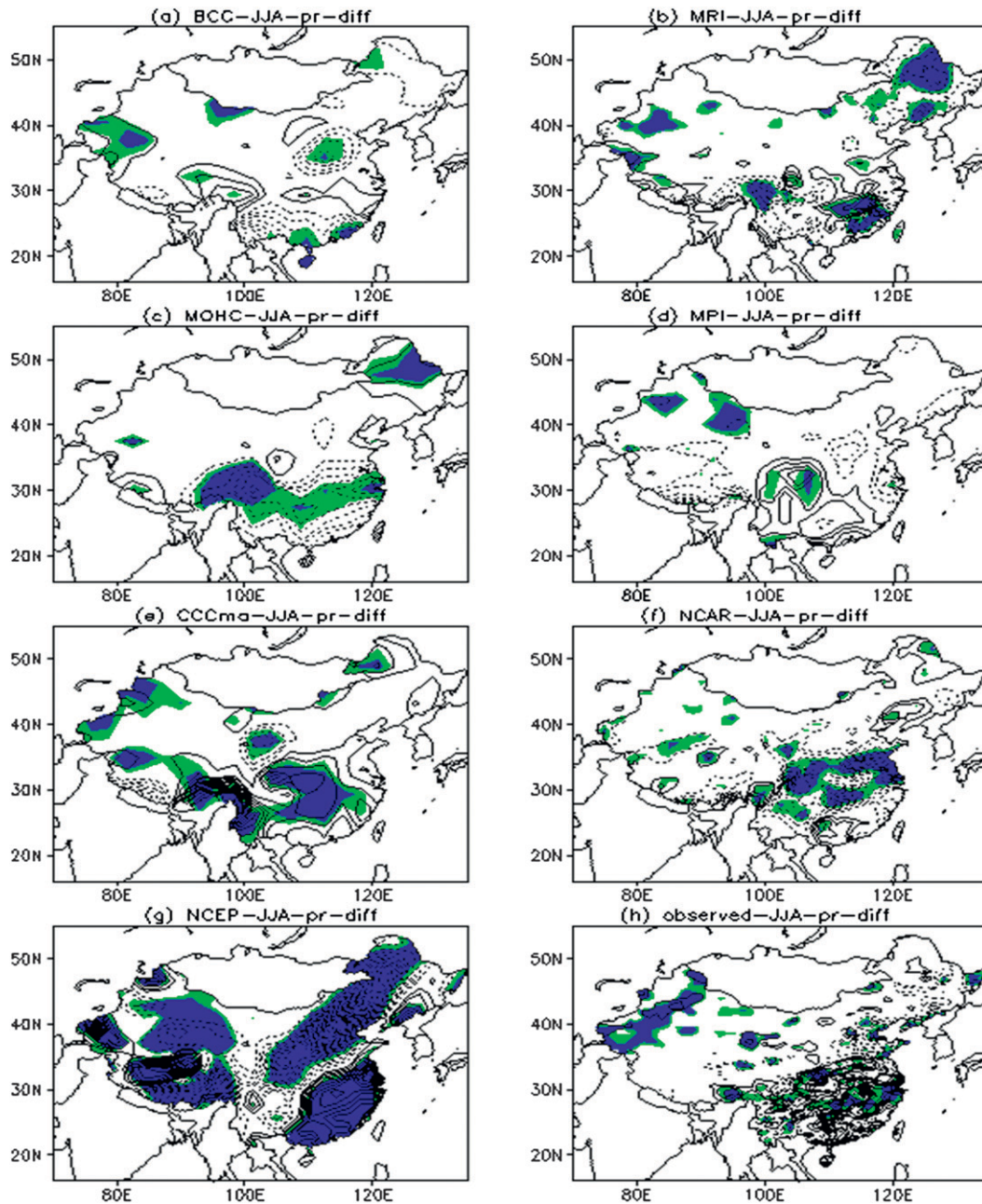


FIG. 2. Differences of summer averaged precipitation over China between 1990–2005 and 1960–75 for (a) BCC, (b) MRI, (c) MOHC, (d) MPI-M, (e) CCCma, (f) NCAR, (g) the NCEP–NCAR reanalysis, and (h) observations. The contour interval is $20 \text{ kg m}^{-2} \text{ summer}^{-1}$. The solid (dashed) lines are positive (negative) composite values. The shadings denote the significance of differences at the 90% (green) and 95% (blue) confidence levels by the Student's t test, respectively.

b. T_s over the boreal mid- to high latitudes and the Arctic

The six models can approximately simulate the averaged T_s variation tendency over the Arctic ($65^\circ\text{--}90^\circ\text{N}$) in winter (December–February), spring (March–May) and

summer (June–August) and the abrupt temperature increases over the Arctic that occurred at the end of the 1970s (not shown). The composite patterns of T_s for the winter (not shown), spring, and summer from the NCEP–NCAR reanalysis (Figs. 3g, 4g) show that interdecadal temperature increases are more noteworthy in winter and

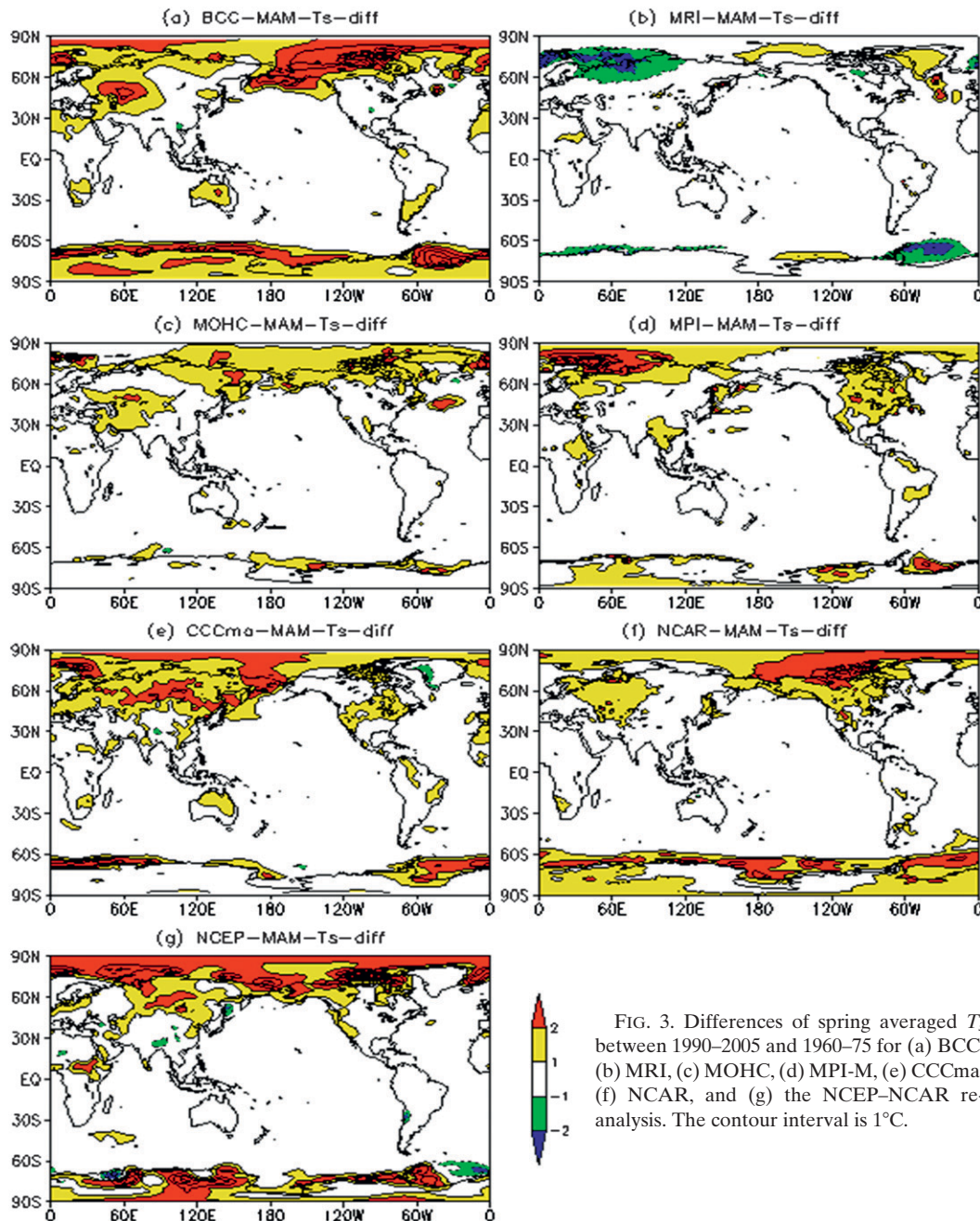


FIG. 3. Differences of spring averaged T_s between 1990–2005 and 1960–75 for (a) BCC, (b) MRI, (c) MOHC, (d) MPI-M, (e) CCCma, (f) NCAR, and (g) the NCEP–NCAR reanalysis. The contour interval is 1°C .

spring than summer over the boreal mid- to high latitudes and the Arctic during 1990–2005 relative to 1960–75. The interdecadal enhancement of T_s can be simulated by BCC, MOHC, MPI-M, CCCma, and NCAR to different extents. The significance for all regions with obvious temperature variations (shaded) can reach and even exceed the 95% confidence level by the Student's t test. The confidence levels are not shown in Figs. 3 and 4 for clarity.

The increases of winter T_s (not shown) are more obvious over the boreal high latitudes and the Arctic in

BCC, MOHC, CCCma, and NCAR than the NCEP–NCAR reanalysis, whose T_s is class B data (Kalnay et al. 1996). The simulated winter T_s increase patterns are generally similar to that of the NCEP–NCAR reanalysis, which is almost symmetrical between the eastern hemisphere and western hemisphere over the boreal mid- to high latitudes in the six simulations and reanalysis. But the regions with obvious T_s increase are larger over the eastern hemisphere than the western hemisphere for CCCma, MPI-M, and the reanalysis, while the T_s

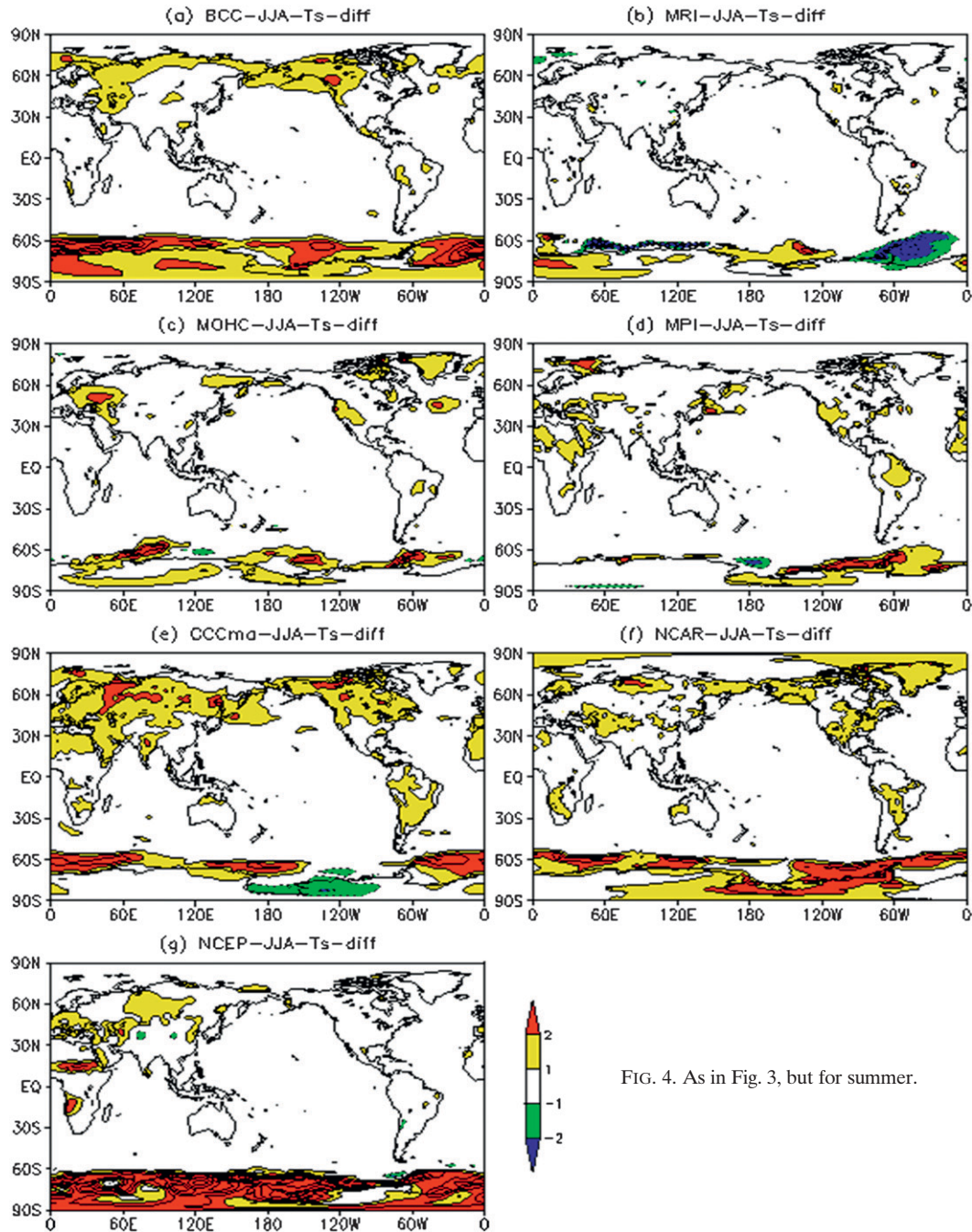


FIG. 4. As in Fig. 3, but for summer.

increase centers are shifted toward the mid- to high latitudes of North Pacific and North America for BCC and NCAR in spring (Fig. 3). MRI has the smallest range of T_s increase among the models; it simulated warming in T_s in the winter (not shown), but T_s even decreases in spring (Fig. 3b) over the mid- to high latitudes of Eurasia. In summer (Fig. 4), obvious T_s enhancement occurs mainly over the mid- to high latitudes (but not much over the Arctic) for BCC and CCCma,

while the T_s increase is not notable for MRI, MOHC, and MPI-M. The summer T_s increase mainly covers the midlatitudes of Eurasia in the NCEP–NCAR reanalysis. Thus, the T_s increase moves moderately toward the south and is reduced in amplitude from winter and spring to summer.

Li and Leung (2013) discussed the role of the increase of spring Arctic T_s and its impact on the interdecadal Asian summer monsoon. Although the T_s increases over

other regions can also have important impacts on Asian summer monsoon precipitation (Li et al. 2010), the T_s increases of the boreal mid- to high latitudes and the Arctic are more notable than that over the tropics and subtropics (Figs. 3, 4). The distributions of anomalous thermal energy and latitudinal imbalance must have some impact on the global climate variations. In what follows, we focus on the direct and indirect impact of the interdecadal T_s variation over the boreal mid- to high latitudes on the summer precipitation over the YRV and assess the ability of the six models to capture such relationships.

4. Regressions of interdecadal winter, spring, and summer T_s on the summer precipitation over the YRV

Our recent study has demonstrated the effective correlation (significance reaching or exceeding the 95% confidence level) between the leading modes of interdecadal summer precipitation over China and the spring T_s of the Arctic, which is positive (negative) for the precipitation over the YRV and south China (north China) (Li and Leung 2013). In this section, we continue to explore the relationship using the six model simulations and the NCEP–NCAR reanalysis. From the observed interdecadal variations of precipitation over China (Fig. 2h), the interdecadal increase of precipitation occurred mainly over the YRV in 1990–2005 relative to 1960–75. Therefore, the regression and correlation analyses are directly carried out between the interdecadal variations of summer precipitation over the YRV and the winter, spring, and summer T_s over the boreal mid- to high latitudes and the Arctic during 1956–2005 with a one-dimensional Gaussian low-pass filter (temporal scale of 9 yr and longer) at every grid point.

Regressions of the interdecadal variation of winter (not shown), spring, and summer T_s over the mid- to high latitudes and the Arctic (45° – 90° N) onto the interdecadal variation of summer precipitation over the YRV are shown in Figs. 5 and 6. The high positive correlations and regressed T_s values over the boreal mid- to high latitudes are basically captured by MPI-M and CCCma (Figs. 5d,e and 6d,e), which are similar to those reported in our previous study (Li and Leung 2013) about the interdecadal relationship between the summer precipitation over the YRV and the spring T_s using the twentieth-century reanalysis data. However, only CCCma can simulate the noteworthy winter, spring, and summer correlations over the mid- to high latitudes of Asia and the Arctic consistently (contrast Figs. 5e and 6e to Figs. 5d and 6d). Although the high correlation and strong regressed T_s are also prominent in MPI-M, they

are absent over the mid- to high latitudes of Asia (around Lake Baikal) in winter and spring and over the Arctic in summer. It is interesting to recall from Fig. 2 that only CCCma can approximately capture the interdecadal enhancement of precipitation over the YRV (Fig. 2e) while MPI-M partly simulated the interdecadal increase in some areas (Fig. 2d).

Positive regressed T_s and correlation are partly simulated by MRI (Figs. 5b, 6b), but high anticorrelations and low regressed T_s in winter and spring are found in BCC, MOHC, and NCAR (Figs. 5a,c,f and Figs. 6a,c,f). So although MRI cannot simulate the interdecadal variation of T_s better than BCC, MOHC, and NCAR (Fig. 3), it can partly capture the relationship between the summer precipitation over the YRV and T_s over the mid- to high latitudes in winter and spring. Correspondingly, MRI can partially capture the interdecadal increase of precipitation over the YRV (Fig. 2b). The NCEP–NCAR reanalysis and observed precipitation show that only the regressed spring T_s over the Arctic is important for the summer precipitation (Figs. 5g,h). We note, however, that the precipitation and T_s are class C and B data, respectively, in the NCEP–NCAR reanalysis (Kalnay et al. 1996), and the regressed values of interdecadal T_s are very small in winter, spring, and summer.

Overall, the results reported suggest that the ability to simulate consistent interdecadal variations of T_s over the Arctic and the boreal mid- to high latitudes in winter, spring, and summer is important for successful simulation of the interdecadal variations of the summer precipitation over the YRV. To explore mechanisms that may link the warming in the Arctic and the boreal mid- to high latitudes to summer precipitation over the YRV, we analyze the atmospheric circulation associated with summer precipitation over the YRV (section 5) and investigate the links between the anomalous circulation and T_s over the Arctic and boreal mid- to high latitudes (section 6).

5. Correlation between the summer precipitation over the YRV and atmospheric circulation

a. Correlations with zonal and meridional wind components and vertical airflow over eastern Asia

Atmospheric circulation has a dominant control on moisture convergence and precipitation over the YRV. Analysis of winds and moisture transport shows that all models can simulate the basic climatological patterns over East Asia. Even the differences between the two periods before and after the decadal shift are very similar over eastern China, except for MRI. Previous studies comparing observations and simulations suggested that a good model at simulating the regional precipitation

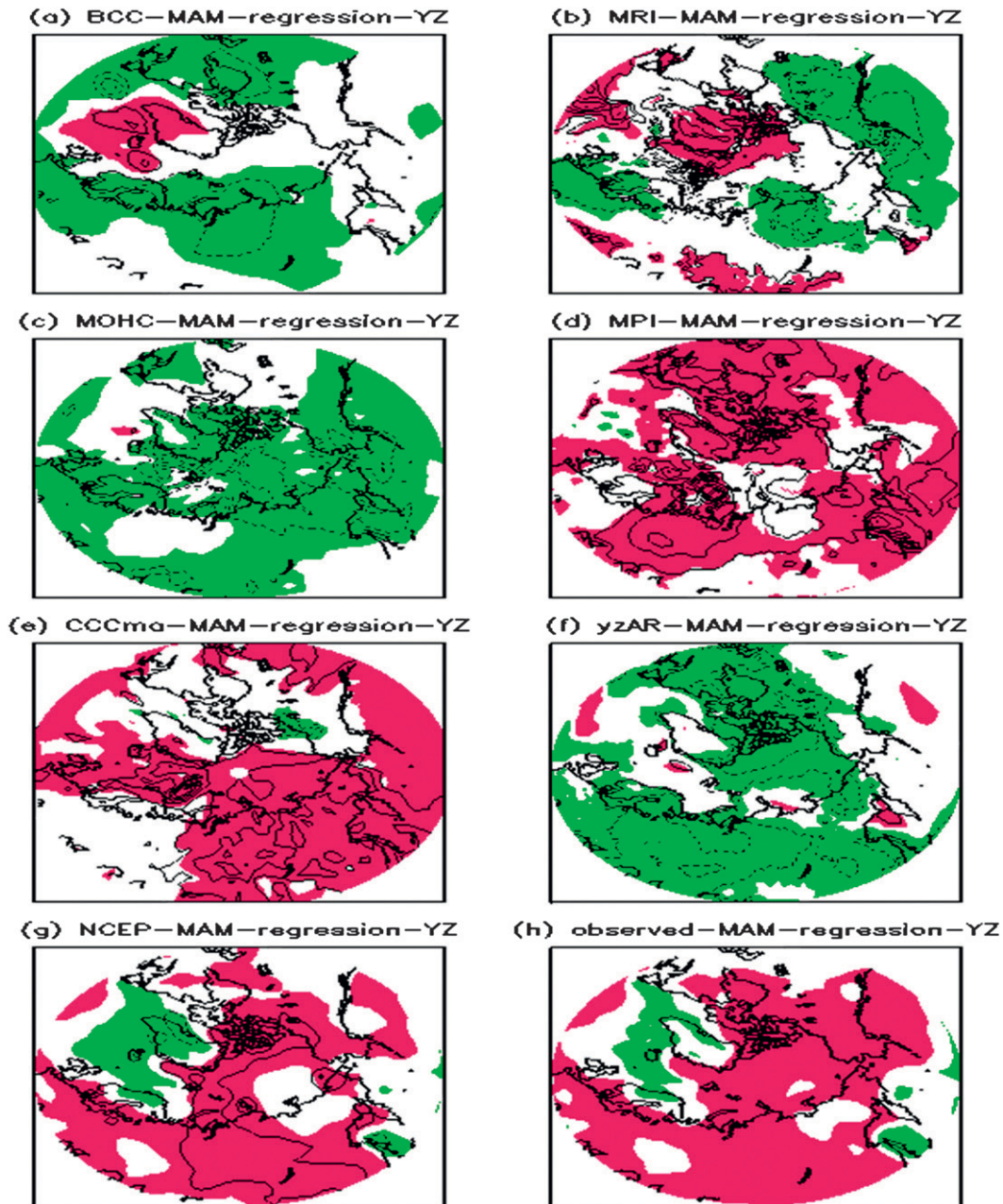


FIG. 5. The regressed anomalous spring T_s with reference to the time series of the interdecadal summer precipitation over the YRV during 1956–2005 for (a) BCC, (b) MRI, (c) MOHC, (d) MPI-M, (e) CCCma, (f) NCAR, (g) the NCEP–NCAR reanalysis, and (h) T_s from the NCEP–NCAR reanalysis and observed precipitation. The contour interval is 0.01. Shading indicates areas where the correlation coefficients are statistically significant at the 95% confidence level (red is $\geq +0.27$, green is ≤ -0.27).

over eastern China during the rainy seasons should have 1) a good relationship between precipitation and low-level meridional wind and 2) a good capability in simulating the observed meridional wind feature. This raises the issue of the importance of low-level wind simulations to improvements of regional precipitation simulations

(Zeng et al. 2012). Also from the previous studies, we know that summer monsoon precipitation events over eastern China are often accompanied by the intersection and convergence of southerly and northerly (i.e., meridional wind convergence) and/or zonal wind shear in the lower troposphere and divergence in the upper

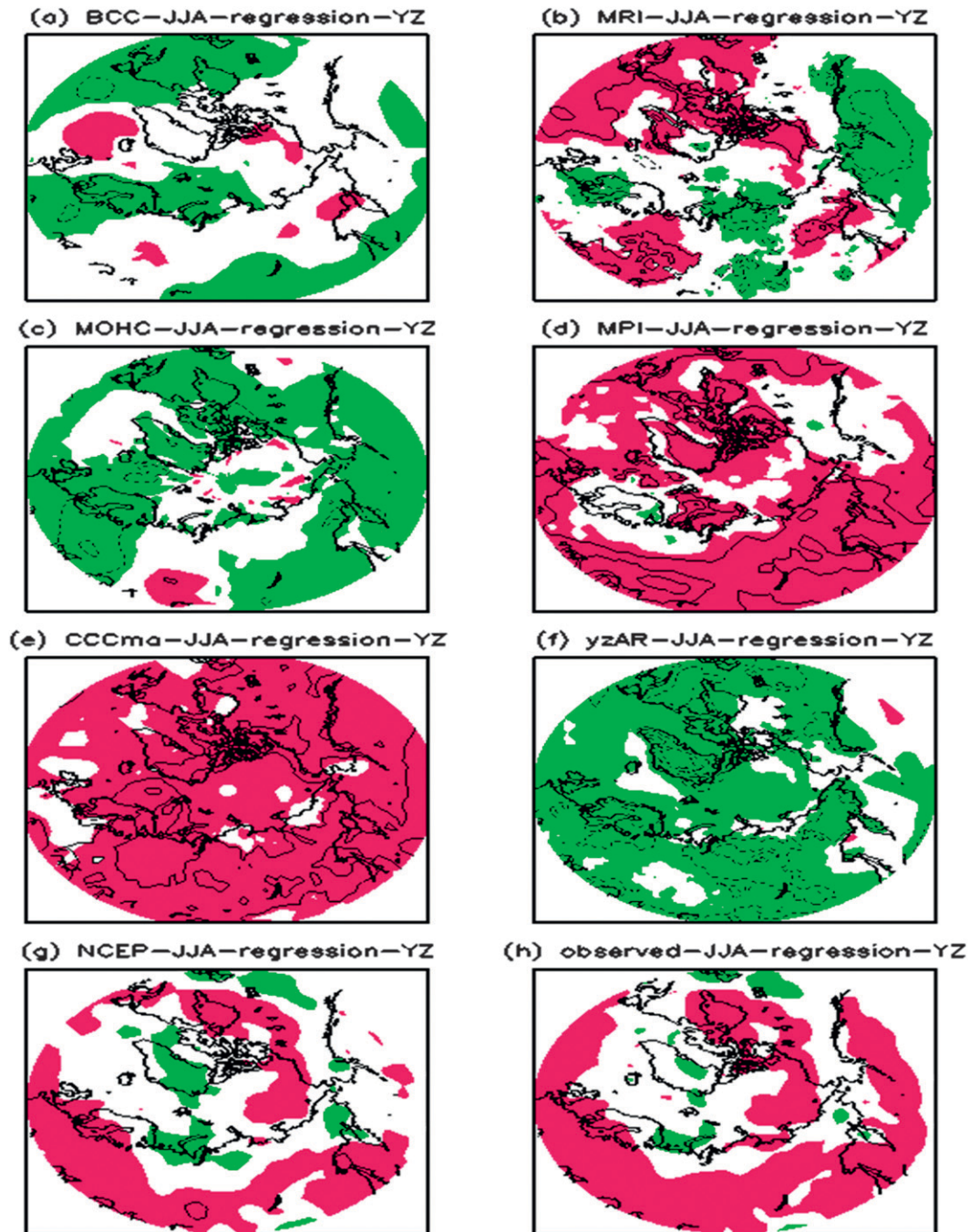


FIG. 6. As in Fig. 5, but for summer.

troposphere. Although Li et al. (2010) pointed out that a model that successfully reproduces the monsoon circulation does not always have a successful reproduction of rainfall anomalies, correct simulation of the relationship between precipitation and wind field at the lower and upper troposphere is a necessary, if not sufficient, condition for simulating the summer monsoon precipitation over eastern China.

Figure 7 shows the contemporaneous correlations between the summer precipitation over the YRV (100° – 120° E, 27° – 33° N) and both zonal (green is positive for westerly) and meridional (red is positive for southerly) winds at 850 hPa during 1956–2005 from the six model simulations (Figs. 7a–f), NCEP–NCAR reanalysis winds and precipitation (Fig. 7g), and NCEP–NCAR winds with observed precipitation (Fig. 7h). Dipoles of positive

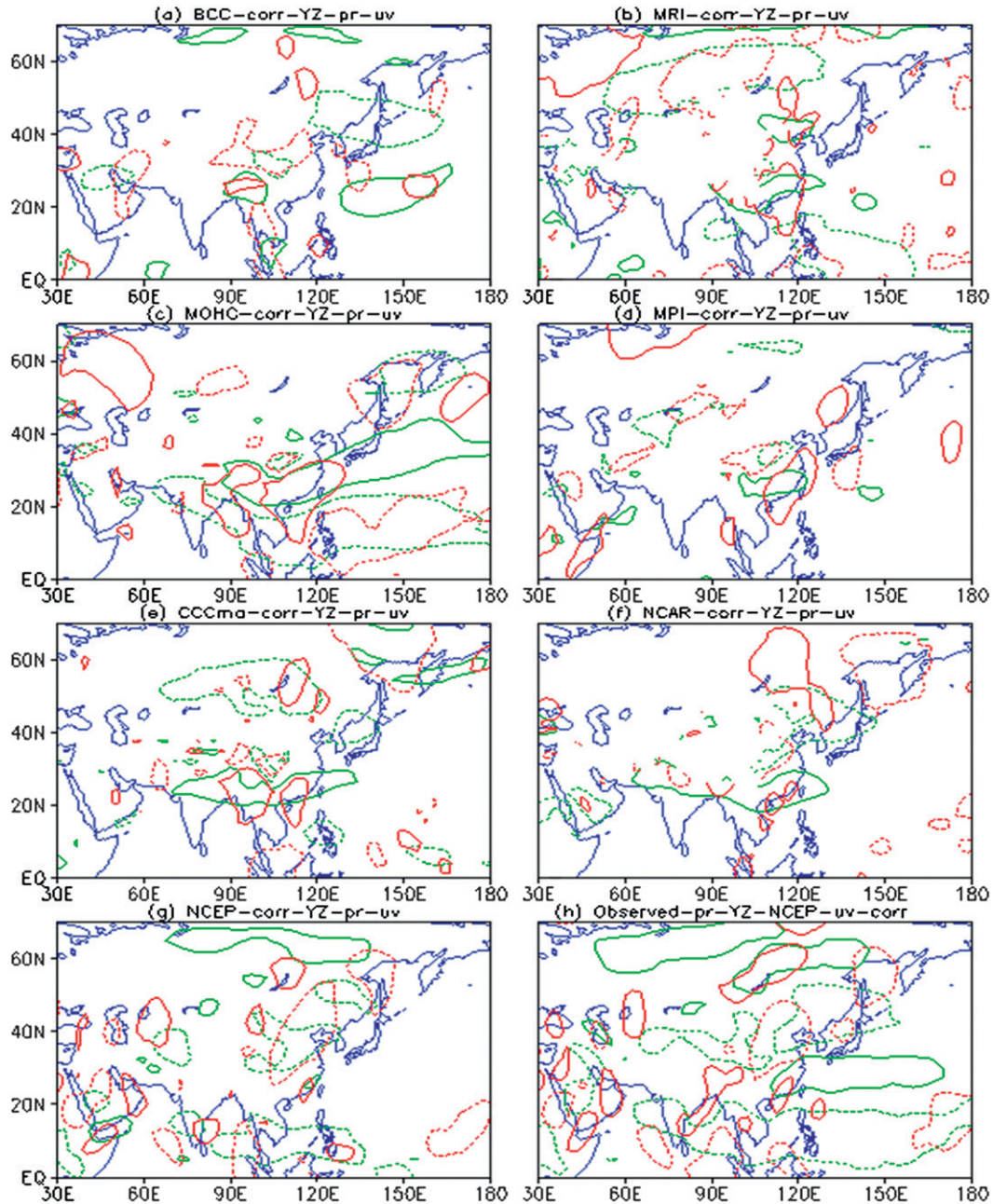


FIG. 7. Correlations between the summer precipitation over the Yangtze River valley and zonal wind (green) and meridional wind (red) at 850 hPa from 1956 to 2005 for (a) BCC, (b) MRI, (c) MOHC, (d) MPI-M, (e) CCCma, (f) NCAR, (g) the NCEP-NCAR reanalysis, and (h) observations; u and v are from the NCEP-NCAR reanalysis and observed precipitation. The circle areas show the significance exceeding the 95% confidence level. Solid and dashed lines show positive and negative values, respectively.

(solid) and negative (dashed) values in green and red indicate zonal wind shear and meridional wind convergence, respectively. Figure 7 reveals reasonably the contributions of zonal shear and meridional convergence over eastern China simulated by MOHC, MPI-M, CCCma, and NCAR (Figs. 7c–f). Correlation analyses using the

NCEP-NCAR reanalysis winds and observed precipitation (Fig. 7h) demonstrate similar relationships. For CCCma (Fig. 7e), the northerly (dashed red) and easterly (dashed green) components that correlate with precipitation (Fig. 7e) tend to be more westward than the NCEP-NCAR reanalysis (u and v are class A data; Kalnay et al.

1996) and observed precipitation (Fig. 7h). For BCC (Fig. 7a), precipitation over the middle and lower reaches of the YRV is not supported by southerly and westerly components over south China, but rather, mainly by the southwest wind over the TP. Hence, the zonal wind shear and meridional convergence are located more westward. For MRI (Fig. 7b), the simulated precipitation over the YRV lacks correlation with zonal shear and meridional convergence (i.e., no clear dipole patterns). This partly explains the limited summer precipitation over the YRV simulated by this model (Fig. 1b).

Figure 8 shows the latitude–height section of the correlations between summer precipitation over the YRV and meridional (red is positive for southerly) and vertical airflow (blue is positive for downward) at 100°–120°E from 1956 to 2005. The matching relationship between precipitation and the southerly wind in the lower troposphere, the northerly wind in the upper troposphere, and upward flow are all captured to some extent by MRI, MOHC, MPI-M, CCCma, and NCAR. The upward airflows tend to be northward relative to the low-level southerly wind and upper-level northerly wind in the simulations. The northerly winds at the low-level troposphere are weaker in CCCma and MRI because the convergence is more westward in CCCma and MRI lacks northerly wind at 100°–120°E. In addition, from the vertical airflow patterns, MOHC and NCAR can simulate an opposite phase relationship of precipitation between the YRV (updraft) and south China (downdraft) (Figs. 8c,f), which represents the first mode of the unfiltered summer precipitation over China (Li and Leung 2013).

b. Interdecadal variations of blockings over the mid- to high latitudes of Eurasia

The summer precipitation over the YRV is impacted by many factors, including the mid- to high-latitude blocking highs. We use the definition of the Eurasian blockings discussed by Li and Ding (2004) within the region spanning 20°–160°E and 45°–75°N. The blockings of the Ural Mountains are located at around 40°–70°E, 45°–75°N; the blockings of Lake Baikal are at 90°–140°E, 45°–75°N; and the blockings of the Sea of Okhotsk are at 140°–160°E, 45°–75°N. All of them can have important impacts on the summer precipitation over the YRV (Li and Ding 2004).

The intensities of H500 over mid- to high-latitude Eurasia are mostly enhanced in the summers of 1990–2005 relative to the summers of 1960–75 (Fig. 9), which are clearly simulated by BCC (Ural), MOHC (Ural and Okhotsk), MPI-M (Okhotsk), and CCCma (Ural, Baikal, and Okhotsk). However, the variation patterns of H500 are different from one another. For example, the interdecadally intensified blockings are located from the Ural

Mountains to the Sea of Okhotsk (with a notable closed center) in CCCma (Fig. 8e), which exceeds the 95% confidence level using the Student's *t* test. For BCC, MRI, MOHC, MPI-M, and NCAR, the interdecadally intensified blockings lack a closed center over Lake Baikal (Figs. 9a–f). The center of the interdecadally intensified blocking is located over Lake Baikal from the NCEP–NCAR reanalysis (Fig. 9g). In other words, only CCCma can simulate the interdecadal enhancement of summer blocking over Lake Baikal found in the NCEP–NCAR reanalysis. Furthermore the blocking enhancement is maintained from winter (not shown) to summer by both CCCma and the NCEP–NCAR reanalysis, except that the center in CCCma moves moderately from around Lake Baikal in winter to around the Sea of Okhotsk in spring and then expands to include the Ural Mountains, Lake Baikal, and the Sea of Okhotsk in summer (Fig. 9e), while the center is held persistently at Lake Baikal from winter to summer in the NCEP–NCAR reanalysis.

The zonal distribution of interdecadal variation of geopotential height between 1990–2005 and 1960–75 in Asia (60°–160°E) shows enhanced H500 over the low to middle latitudes (0°–60°N) in MPI-M and NCAR (not shown), and the H500 enhancement even stretches and extends beyond 60°N by MOHC and CCCma at the mid- and upper-level troposphere. Furthermore, CCCma and MOHC can simulate the intensified centers at the mid- and upper troposphere in the mid- to high latitudes (45°–75°N), especially CCCma. The NCEP–NCAR reanalysis shows the intensified center located throughout the troposphere. In addition, the strengthened highs beyond 60°N started in spring in MOHC and CCCma (not shown). However, BCC, MRI, MPI-M, and NCAR lack the enhancement in the mid- and upper-level troposphere between 45° and 75°N.

c. Correlations with H500

Correlation analyses show that summer precipitation over the YRV are often accompanied by the Ural blocking in MRI (Fig. 10b); the Ural, Baikal, and Okhotsk blockings in MPI-M [but the zonal ranges and locations are different from the definition of Li and Ding (2004)] (Fig. 10d); and the Baikal and Okhotsk blockings in CCCma (Fig. 10e), with significances exceeding the 95% confidence level. Correlation analysis between observed precipitation and H500 of the NCEP–NCAR reanalysis reveals that precipitation over the YRV is often accompanied by the Baikal and Okhotsk blockings (Fig. 10h). Pu et al. (2008) and Ma et al. (2012) verified a prominent meridional teleconnection mode that displays a positive–negative–positive height anomaly from north to south along the east coast of East Asia at

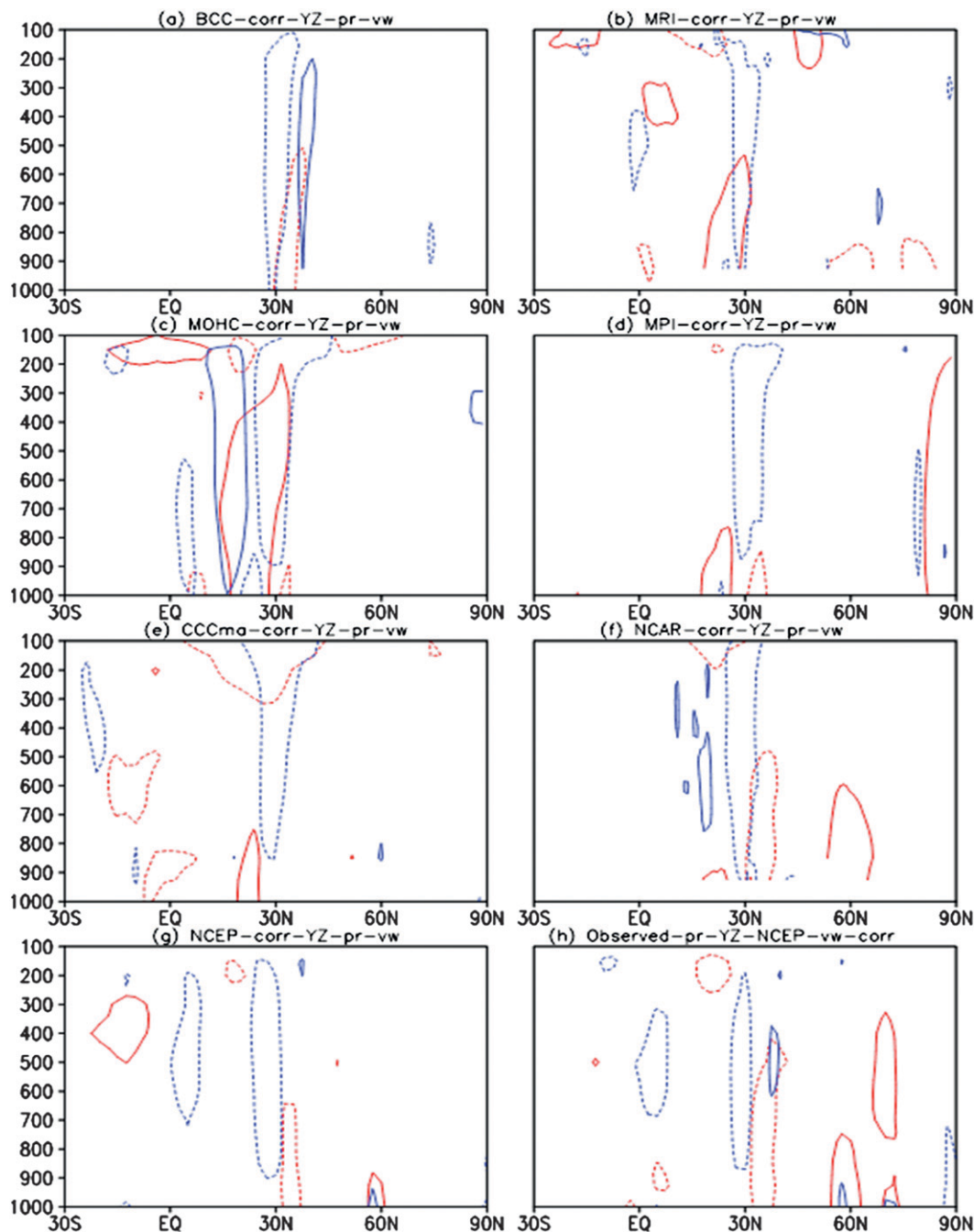


FIG. 8. As in Fig. 7, but for the latitude–height section of correlations between the summer precipitation over the YRV and summer meridional wind (red) and velocity airflow (blue) at 100°–120°E.

500 hPa in summer. This mode reflects the in-phase variations for the Okhotsk blocking and the western subtropical Pacific high (Figs. 10e,h). That is, when the Okhotsk blocking is more intense, the subtropical high tends to be stronger than its climatological average. At the same time, precipitation in the middle and lower reaches of the YRV is above the climatological mean. In

Fig. 10, only CCCma can capture the teleconnection relationship between the summer precipitation over the YRV and H500 over the eastern coast of East Asia to some extent during 1956–2005 (Fig. 10e). This suggests that the teleconnection pattern has some contributions to the summer precipitation over the YRV during 1956–2005, although some parts of the teleconnection pattern

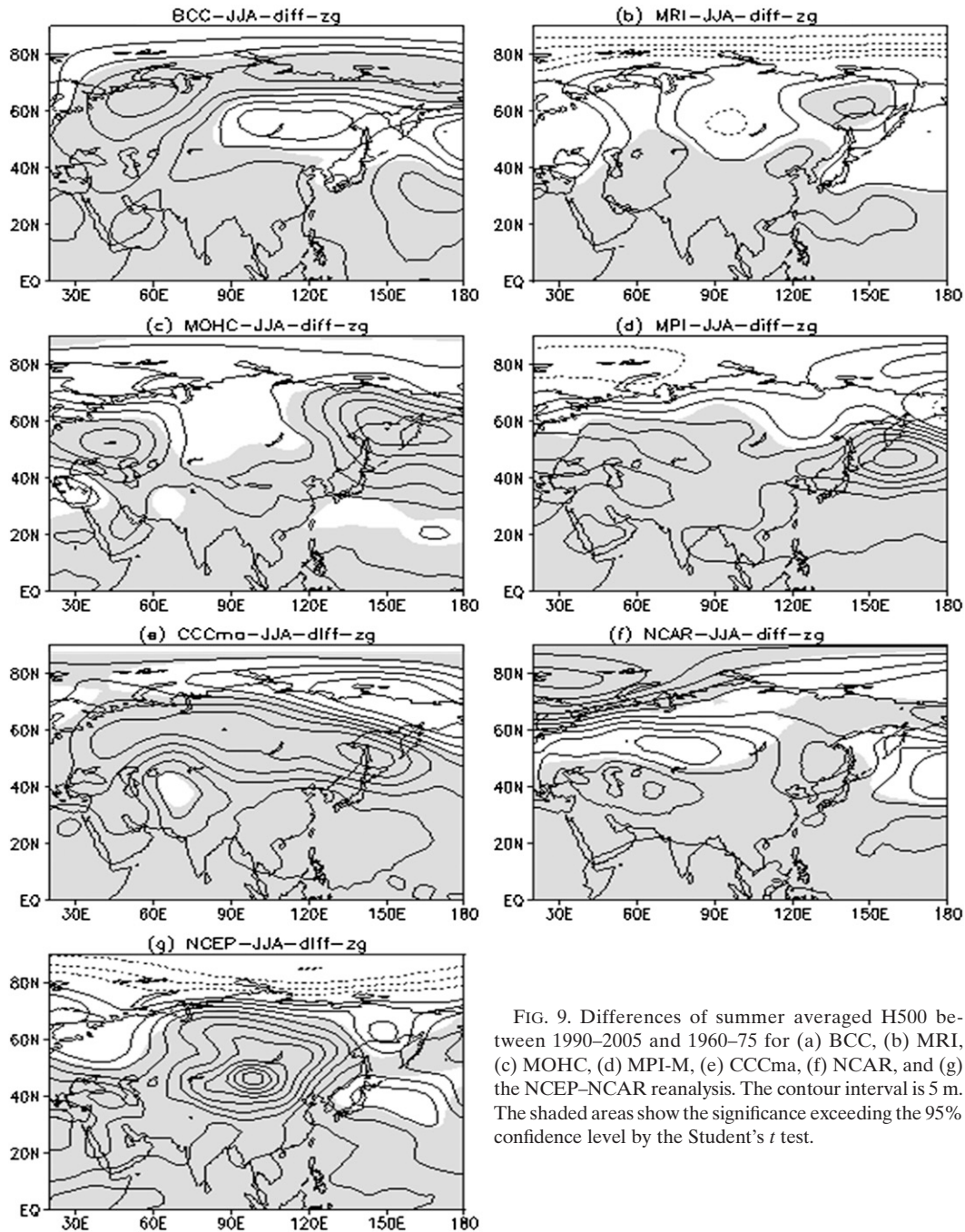


FIG. 9. Differences of summer averaged H500 between 1990–2005 and 1960–75 for (a) BCC, (b) MRI, (c) MOHC, (d) MPI-M, (e) CCCma, (f) NCAR, and (g) the NCEP–NCAR reanalysis. The contour interval is 5 m. The shaded areas show the significance exceeding the 95% confidence level by the Student's t test.

do not exceed the 95% confidence level. This may be because we define the summer to include June, July, and August in the present study, but the summer precipitation over the YRV occurs mainly in June–July (e.g., Ma et al. 2012), so some interference signals may possibly be added to the June–August summer precipitation and circulations (Pu et al. 2008). In addition, Pu et al. (2008) and Ma et al. (2012) derived their teleconnection pattern based on the leading mode, but in the present study, we use the

correlation between the summer precipitation over the YRV and H500 directly without any filter. Thus, the confidence levels of significance are impacted.

The zonal height sections of the correlation analyses between the precipitation over the YRV and 60°–160°E geopotential height field in the troposphere (not shown) show that only CCCma can simulate the close positive relationship at the mid- to upper troposphere of Asia, with significance exceeding the 95% confidence level.

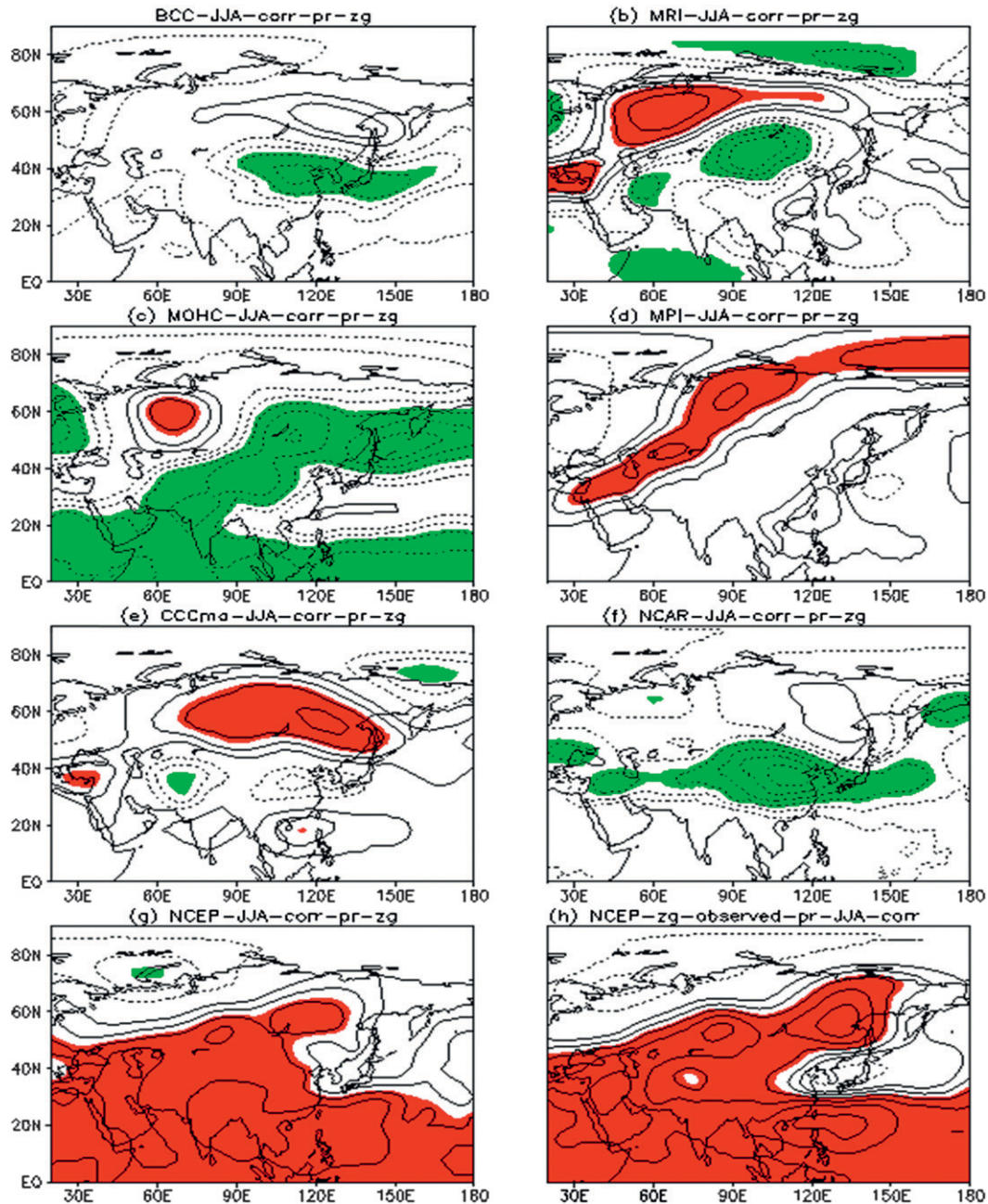


FIG. 10. Correlation between the summer precipitation over the YRV and summer H500 from 1956 to 2005 for (a) BCC, (b) MRI, (c) MOHC, (d) MPI-M, (e) CCCma, (f) NCAR, (g) the NCEP-NCAR reanalysis, and (h) H500 is from the NCEP-NCAR reanalysis and observed precipitation. The contour interval is 0.1. The shaded areas show the significance exceeding the 95% confidence level by the Student's t test.

The pattern is similar to the correlation between observed precipitation and the geopotential height of the NCEP-NCAR reanalysis, but the latter is more southward and at the low to middle troposphere of Asia. MRI is the only other model that also simulated a positive relationship, which is mainly located at the low-level troposphere and more northward than 60°N,

although its significance also reaches the 95% confidence level.

These results suggest that realistic simulations of the interdecadal enhancement of the geopotential height at the mid- to high latitude in 1990–2005 relative to 1960–75 and its link to precipitation over the YRV (Fig. 10e) as well as the blockings over Lake Baikal and the Sea of

TABLE 2. The squared covariances (%) explained by SVD1 (Monte Carlo approach). The squared covariances shown in bold exceed 95% confidence level. DJF is December–February, MAM is March–May, and JJA is June–August.

Simulations and reanalysis	Summer H500 hPa (20°–160°E)	Spring T_s using original order (0°–360°E, 45°–90°N)			Correlation coefficient between the time coefficients of T_s and 500-hPa height			Spring T_s using scrambled order (95% confidence level)		
		DJF	MAM	JJA	DJF	MAM	JJA	DJF	MAM	JJA
BCC	30°–80°N	75	66	56	0.59	0.53	0.85	63	63	55
	0°–80°N	77	70	58	0.64	0.60	0.87	62	63	54
MRI	30°–80°N	54	36	38	0.47	0.52	0.80	54	50	45
	0°–80°N	51	34	36	0.47	0.52	0.80	53	49	43
MOHC	30°–80°N	47	50	42	0.58	0.64	0.92	49	50	38
	0°–80°N	49	51	43	0.59	0.66	0.91	51	48	38
MPI-M	30°–80°N	66	67	43	0.59	0.57	0.86	62	60	42
	0°–80°N	74	72	44	0.67	0.62	0.86	61	60	42
CCCma	30°–80°N	77	61	64	0.74	0.64	0.89	60	54	55
	0°–80°N	80	66	66	0.78	0.67	0.90	61	54	55
NCAR	30°–80°N	58	60	53	0.46	0.52	0.86	63	65	54
	0°–80°N	63	62	52	0.54	0.57	0.86	62	63	52
NCEP–NCAR	30°–80°N	62	73	39	0.67	0.66	0.87	51	63	40
	0°–80°N	66	77	42	0.66	0.66	0.86	53	66	42

Okhotsk at the mid- to upper troposphere are important reasons why CCCma can approximately simulate the interdecadal increase of precipitation over the YRV. If so, what can induce the summer enhanced blockings at the mid- to high latitudes of Asia? To address this question, the relationship among the winter, spring, and summer T_s and blockings at the mid- to high latitudes of Eurasia is investigated in the following section.

6. SVD analyses between T_s and H500

SVD analysis examines the coupled variation of two fields (Bretherton et al. 1992; Wallace et al. 1992; Weng et al. 1999; Li et al. 2009) to help identify only those modes of behaviors in which the variations of two fields are strongly coupled. In our SVD analysis, every principal component is scaled by its standard deviation in the temporal domain, the corresponding spatial pattern is multiplied by the standard deviation, and only the first leading mode (SVD1) is analyzed. The spatial pattern is shown corresponding to its positive time coefficient. The confidence level of SVD1 is assessed by testing the significance of their squared covariance associated with the first leading mode using the Monte Carlo approach (Venegas et al. 1996; Peng and Fyfe, 1996; Li et al. 2009). The SVD analysis is repeated 100 times, linking the original H500 with the scrambled mid- to high-latitude T_s to remove the chronological order between T_s and H500 while the T_s spatial structure within each year is preserved. Moreover, we skipped every other grid point for NCAR and MRI because their higher horizontal resolutions require more computational time to test significance. Limited experiments confirm that the

spatial patterns, time evolutions, and squared covariances of SVD1 obtained with the skipping point method are almost identical to those using data with full resolution.

SVD analysis is carried out between the winter, spring, or summer T_s at 0°–360°E, 45°–90°N and summer H500 at 20°–160°E, 30°–80°N or 20°–160°E, 0°–80°N during 1956–2005 (Table 2). The spatial patterns and time evolutions of SVD1 are preserved, regardless of whether H500 at 20°–160°E, 30°–80°N or H500 at 20°–160°E, 0°–80°N is considered. Only the squared covariances and the coefficients between the time coefficients of T_s and H500 are somewhat altered (Table 2). Moreover, the squared covariances of SVD1 between the summer T_s and the summer H500 are the minimum for most simulations and the NCEP–NCAR reanalysis, but the correlation coefficients between the time coefficients of the summer T_s and the summer H500 are the maximum across all datasets. This reveals the complexities of spatial modes and the consistency of time evolutions for the first leading mode of the summer T_s and H500. We also performed SVD analyses for winter T_s and winter H500, winter T_s and spring H500, and spring T_s and spring H500 using the six model simulations and the NCEP–NCAR reanalysis (not shown in Table 2) to compare all of the first modes among the couplings in different seasons (except autumn) for a comprehensive understanding.

Section 5 shows that the Baikal and Okhotsk blockings have important contributions to the interdecadal increase of precipitation over the YRV (Figs. 10e,h). From Table 2, the coupled relationships between the winter, spring, or summer T_s and summer H500 exceed the 95% confidence level in BCC, MPI-M, and CCCma.

Thus, we need to explore why CCCma can approximately simulate the interdecadal enhancement of the Baikal and Okhotsk blockings while BCC and MPI-M cannot produce similar variations from the coupled relationship between T_s and H500.

- 1) Winter T_s –winter H500 (not shown): The SVD1 spatial patterns of T_s and H500 for BCC (69%), MPI-M (76%), CCCma (58%), and the NCEP–NCAR reanalysis (51%) are similar to one another. They all demonstrate positive anomalies in H500 over Baikal and Okhotsk when T_s is enhanced over Baikal, but T_s is mostly reduced in other boreal mid- to high latitudes. However, only the squared covariance of the MPI-M SVD1 reaches the 95% confidence level, so the coupled leading modes are unstable or uncertain in BCC and CCCma as well as the NCEP–NCAR reanalysis.
- 2) Winter T_s –spring H500 (not shown): The SVD1 spatial patterns of winter T_s and spring H500 for BCC (53%), MPI-M (72%), CCCma (66%) and the NCEP–NCAR reanalysis (55%) are again similar to one another, which shows that warmer T_s over most of the boreal mid- to high latitudes corresponds to positive H500 anomalies over the mid- to high latitudes of Eurasia. For the NCEP–NCAR reanalysis, the center of the positive H500 anomalies is located over Baikal. Moreover, the time evolutions of SVD1 display the same interdecadal phase for BCC, MPI-M, CCCma, and the NCEP–NCAR reanalysis. The squared covariances of MPI-M, CCCma, and the NCEP–NCAR reanalysis exceed the 95% confidence level but not BCC.
- 3) Winter T_s –summer H500: From Table 2, the squared covariances of the first leading coupled modes between the winter T_s and summer H500 exceed the 95% significance level for BCC, MPI-M, CCCma, and the NCEP–NCAR reanalysis. However, the spatial patterns of H500 are not reasonable, as the centers of the blockings tend to decrease from outside to inside over Baikal and Okhotsk in BCC and MPI-M (not shown). Only CCCma and the NCEP–NCAR reanalysis show reasonable coupled spatial modes of T_s and H500, with increase in H500 over Baikal corresponding to warmer T_s over most of the boreal mid- to high latitudes (Fig. 11). The same phase variations of T_s are found around Baikal and most other boreal mid- to high latitudes. From the time evolution of SVD1 (Figs. 11c1,c2), the interdecadal variation is in negative (positive) phase during 1960–75 (1990–2005) in CCCma and the NCEP–NCAR reanalysis.
- 4) Spring T_s –spring H500 (not shown): The squared covariances of SVD1 do not reach the 95% confidence

level in BCC, MPI-M, CCCma, and the NCEP–NCAR reanalysis together. All the T_s spatial patterns show an opposite phase between Baikal and other boreal mid- to high latitudes in BCC, MPI-M, and CCCma, but not the NCEP–NCAR reanalysis.

- 5) Spring T_s –summer H500: Table 2 shows that the squared covariances of SVD1 exceed the 95% confidence level in BCC, MPI-M, CCCma, and the NCEP–NCAR reanalysis. However, the centers of the blockings tend to diminish from outside to inside over Baikal and Okhotsk in BCC and MPI-M again. CCCma and the NCEP–NCAR reanalysis show reasonable coupled spatial modes with positive anomalies of H500 around Baikal corresponding to warmer T_s over most of the boreal mid- to high latitudes (Fig. 12). From the interdecadal variation of spring T_s (Fig. 3e,g) and the time evolution of SVD1 (Fig. 12c1,c2), CCCma can approximately simulate the variation similar to the NCEP–NCAR reanalysis. The positive and negative phases are corresponding to 1990–2005 and 1960–75, respectively.
- 6) Summer T_s –summer H500: The SVD1 spatial patterns of T_s and H500 show positive anomalies of H500 that tend to decrease from outside to inside over Lake Baikal and Okhotsk in MPI-M reaching some negative values at the center in BCC, which correspond to warmer T_s over most of boreal mid- to high latitudes. For CCCma (Fig. 13), the positive anomalies of H500 around Ural, Baikal, and Okhotsk correspond to warmer T_s over most of boreal mid- to high latitudes. Although the positive H500 anomalies have no obvious center over Baikal, the positive anomalous band stretches across Ural, Baikal, and Okhotsk, resembling the NCEP–NCAR reanalysis.

The above analyses for CCCma and the NCEP–NCAR reanalysis demonstrate that the summer H500 variation over Baikal and Okhotsk has a close relationship with the winter, spring, and summer T_s spatial distribution and interdecadal variation over most of the boreal mid- to high latitudes. At the same time, the same phase of the interdecadal T_s variation is maintained between the mid- to high latitudes of Asia (around Baikal) and most of the other boreal mid- to high latitudes. Therefore, we speculate that BCC and MPI-M cannot effectively simulate the enhancement of the Baikal and Okhotsk blocking during 1990–2005 (Figs. 9a,d) because the T_s interdecadal enhancements over the mid- to high latitudes of Asia are insignificant (contrast Figs. 3a,d to Figs. 3e,g, respectively) or the interdecadal T_s in the mid- to high latitudes of Asia (around Baikal) and most of the other boreal mid- to high latitudes vary in opposite phase in BCC and MPI-M; these models failed to

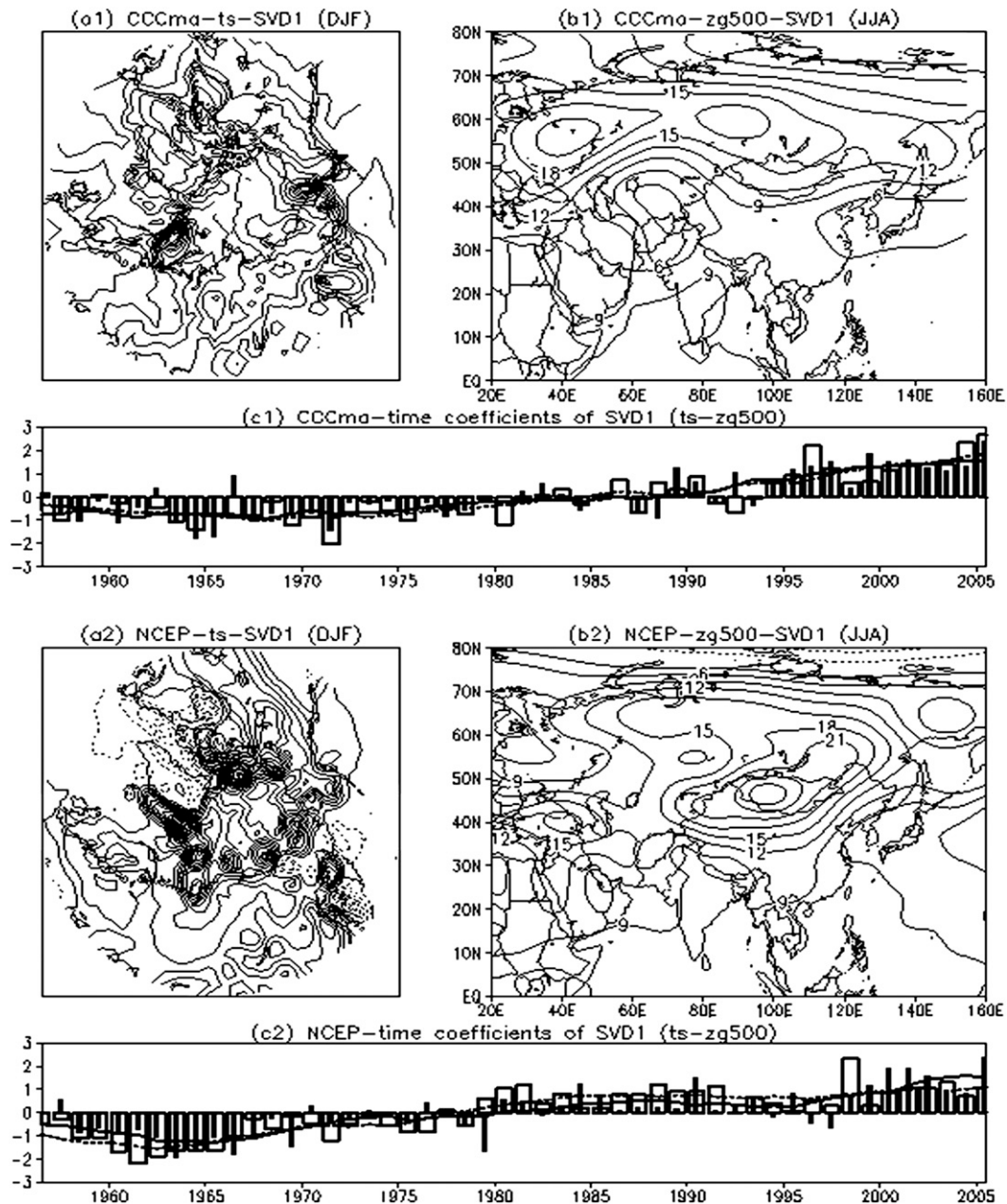


FIG. 11. SVD1 between the winter T_s (0° – 360° E, 45° – 90° N) and summer H500 (20° – 160° E, 0° – 80° N) during 1956–2005. (a1),(a2) The spatial patterns of the T_s anomalies; the contour interval is 0.3° C. (b1),(b2) The spatial patterns of the H500 anomalies; the contour interval is 3 m. (c1),(c2) The corresponding time coefficients for SVD1– T_s (filled bars, solid lines) and SVD1–H500 (unfilled bars, dashed lines) from CCCma and the NCEP–NCAR reanalysis, respectively.

capture the interdecadal anomalies in the Baikal and Okhotsk blockings.

In addition, the squared covariances of the simultaneous correlations do not reach the 95% confidence level between winter T_s and winter H500 or between spring T_s and spring H500 in most simulations and the NCEP–NCAR reanalysis. For the latter, the squared covariance of SVD1 between the summer T_s and summer

H500 is only close to the 95% confidence level (Table 2). This suggests some lag between the warming of T_s over the boreal mid- to high latitudes and the Arctic and the appearance of the anomalous intensified Baikal blocking. This is similar to the conclusion by Arai and Kimoto (2005) that when T_s over Siberia is high in April, blocking events occur more frequently than normal over northeastern Siberia and the Okhotsk Sea in May and June.

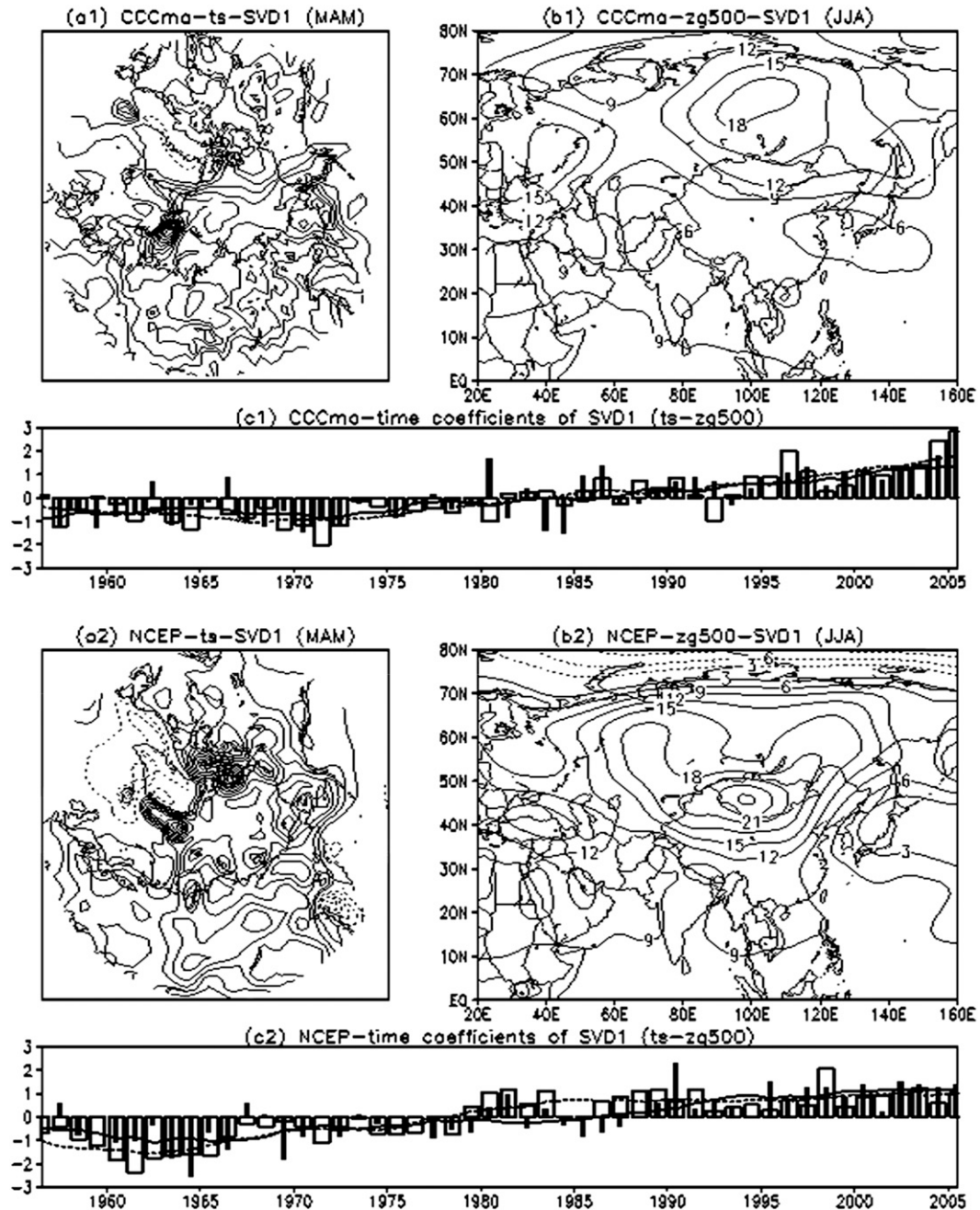


FIG. 12. As in Fig. 11, but for the spring T_s and summer H500.

Associated with the enhanced blocking activity, the early summer precipitation in East Asia will be affected.

7. Mechanisms linking Arctic warming and interdecadal monsoon precipitation

It has been documented that the Arctic climate is rapidly shifting because of the unprecedented warming of the

atmosphere, ocean, and land. Sea ice is a critical component of the Arctic's marine system, but it has consistently declined in all months of the year and since the early 1990s the retreat has been accelerating (Budikova 2009; Wu et al. 2009a,b). Arctic sea ice has the capacity to significantly mediate the exchange of radiation, sensible heat, and momentum between the atmosphere and the ocean, impacting the climate through ice-albedo feedback (Liu and Alexander 2007).

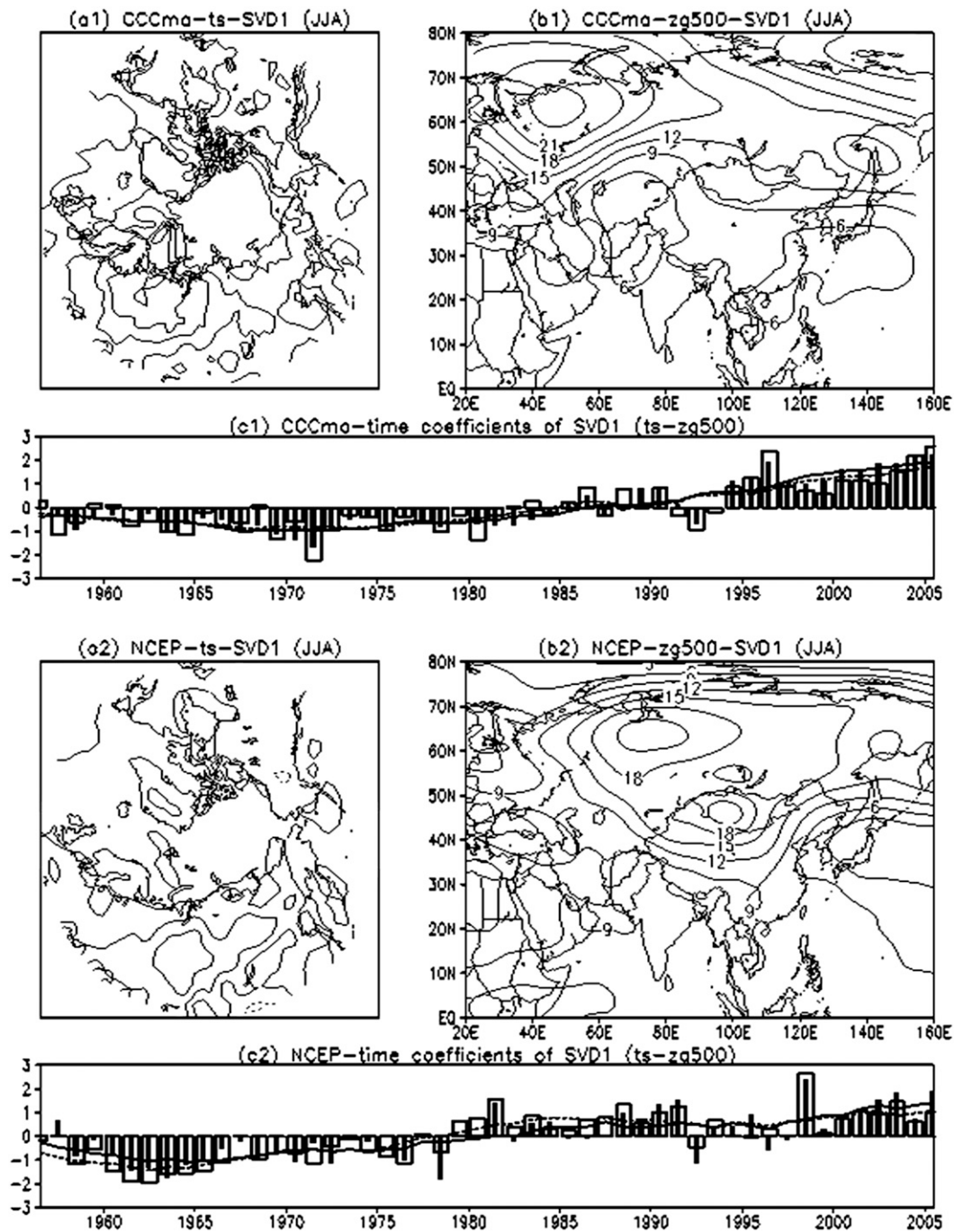


FIG. 13. As in Fig. 11, but for the summer T_s and summer H500.

The reduction of Arctic sea ice concentration is primarily due to the Arctic warming. In the high latitudes, atmospheric warming over the surface expands to the lower latitudes through horizontal advection and eddy transport. Initially, the Arctic surface warming can be more effectively advected to the lower latitudes in areas of northerly flow, as has been observed on the western

sides of the Aleutian and Icelandic lows. This flow is, however, more restricted at the higher latitudes on the eastern sides of pressure systems that prevent the thermal anomalies from being transported south into the midlatitudes (Royer et al. 1990; Dagmar 2009). The general atmospheric circulation processes that dominate over the Eastern Hemisphere limit the advection of

Arctic air southward over the Eurasian continent and inhibit the propagation of anomalous temperatures into the southern latitudes (Royer et al. 1990).

Over the long term, horizontal energy transports within the atmosphere and ocean have to balance the differential radiative heating by the sun (Mayer and Haimberger 2012). The interdecadal warming is more prominent over the high latitudes and the Arctic Ocean in winter and spring (Fig. 3) and the mid- to high latitudes in summer (Fig. 4) than the low latitudes, so the reduced latitudinal temperature gradients (i.e., a decrease in the equator-to-pole thermal gradient) can modify the atmospheric circulation that connects the Arctic to the lower latitudes. Thus, the Arctic warming can result in weakening of the westerlies poleward of 45°N and strengthening of the westerlies in the lower latitudes of the tropical and subtropical regions (Budikova 2009). The weakening of the westerly flow in the midlatitudes has been explained by a concurrent increase in the midtropospheric geopotential heights over the high latitudes and a reduction of the meridional temperature gradient between the high and low latitudes (Budikova 2009).

This study shows that the correlation between T_s and H500 can exceed the 95% confidence level for winter T_s and spring H500, winter T_s and summer H500, and spring T_s and summer H500 in CCCma and the NCEP–NCAR reanalysis. This suggests that the thermal conditions over the boreal high latitudes need some time to dynamically transport or exchange energy with the boreal mid- to high latitudes. When the thermal gradient from equator to pole is reduced, the energy exchange between the high latitudes and the mid- to high latitudes should slow down in the meridional direction before the zonal direction because of Earth's rotation. In addition, consistent T_s variations between Baikal and most of other boreal mid- to high latitudes in winter, spring, and summer appeared to be a necessary condition for the summer blocking to be enhanced and maintained over Baikal. This suggests that the warming over the mid- to high latitudes of Asia alone does not provide sufficient energy to support the summer Baikal blocking enhancement and maintenance. In addition, the relative size of the spatial coverage of the anomalies between the Arctic and the mid- to high latitudes of Asia seems to be very important in deciding the location of blocking. Although we cannot assert that the energy needed to enhance and maintain the blocking over the mid- to high latitudes of Eurasia requires a season to transport from the high latitudes and the Arctic Ocean to the Baikal region, we speculate that the accumulated anomalous energy must reach a certain value to trigger and maintain the stable blocking over the mid- to high latitudes of Asia, so it takes time to cross the accumulated energy threshold.

Specifically, our analyses suggest that the strongest winter warming over most of the boreal high latitudes and the Arctic Ocean may trigger and intensify positive height anomalies over the boreal high latitudes (around the Arctic Ocean), the moderate spring warming could maintain the height anomalies but the central location may be modulated, and lastly the weak summer warming could weaken the positive height anomalies over the mid- to high latitudes of Eurasia, but the positive anomalies across the central band including Baikal still remain.

Our results are consistent with previous studies that demonstrated that the summer blockings over Eurasia are relatively more stable than other seasons and exhibit a distinct interdecadal variation (Zhao and Chen 1990). Furthermore, the Baikal or Okhotsk blocking often corresponds with excessive precipitation over the YRV (Ding and Chan 2005; Wang et al. 2006), and the heaviest precipitation over the YRV during the summer of 1998 coincided with midlevel tropospheric blocking over northeast Eurasia (Okhotsk blocking; Samel and Liang 2003). The westerlies can be separated into two airflows, a southern branch and a northern branch, by the Baikal or Okhotsk blocking. The southern branch can form a large trough over the middle latitudes of Asia so the northwesterly wind behind the trough can intersect the southwesterly and/or southeasterly monsoon flow over the YRV or other regions, depending on the trough extent. This circulation pattern favors the stagnation of the precipitation band in some regions and enhances regional precipitation (Ding and Hu 2003; Ding and Chan 2005). This study demonstrates that CCCma and the NCEP–NCAR reanalysis can approximately simulate the interdecadal enhancement of summer precipitation over the YRV, and they both exhibit relationships between the warming over most of the boreal mid- to high latitudes and the positive anomalies of Baikal blockings while other models that do not capture such relationships also failed to simulate the interdecadal enhancement of summer precipitation over the YRV. Therefore, our analyses suggest that the Baikal blocking may be the bridge that links the warmer winter and spring T_s since the late 1970s to the interdecadal enhancement of summer precipitation over the YRV.

8. Conclusions and discussion

This study focuses on exploring the reasons and mechanisms that induce the interdecadal increase of summer precipitation over the YRV in 1990–2005 relative to 1960–75 and assessing the ability of CMIP5 historical simulations to capture the interdecadal variability. In particular, contributions from the warming of Arctic and mid- to high-latitude T_s , the enhancement of blocking,

and their relationships to interdecadal precipitation variability in the YRV are investigated. The CMIP5 simulations from BCC, MRI, MOHC, MPI-M, CCCma, and NCAR; the NCEP–NCAR global reanalysis; and the observed precipitation of China during 1956–2005 are used in our analyses. Our key findings are summarized below.

- 1) The overall pattern of summer averaged precipitation over China from 1956 to 2005 is captured by BCC, MOHC, MPI-M, CCCma, and NCAR, although the simulated precipitation is generally more prominent over southern and southeastern TP than the observations. Only CCCma can approximately simulate the enhancement of interdecadal summer precipitation over the YRV in 1990–2005 relative to 1960–75. MRI and MPI-M show some signals in limited areas, but MOHC and NCAR exhibit completely opposite interdecadal variations to the observations over the YRV.
- 2) The interdecadal warming of winter T_s can be simulated by BCC, MOHC, MPI-M, CCCma, and NCAR to different extent. However, the dominant centers of spring T_s increase are mainly located in the mid- to high latitudes of Eurasia and the Arctic in MPI-M, CCCma, and the NCEP–NCAR reanalysis, while the centers tend toward the mid- to high latitudes of the North Pacific and North America for BCC and NCAR. In summer, obvious T_s enhancement occurs mainly over the mid- to high latitudes (but not over the Arctic) for BCC, CCCma, and the NCEP–NCAR reanalysis, but MRI shows smaller T_s increases in winter, negative T_s anomalies in spring, and almost invariant T_s in summer over the mid- to high latitudes of Eurasia.
- 3) Regressions of the interdecadal T_s onto the interdecadal summer precipitation over the YRV show that CCCma captures high correlations and strong positive regressed winter, spring, and summer T_s over the boreal mid- to high latitudes of Asia and the Arctic. This suggests that the consistent interdecadal variations of T_s over the Arctic and the mid- to high latitudes of Asia are an important factor for the summer precipitation over the YRV.
- 4) The contemporaneous correlations between the summer precipitation over the YRV and both zonal and meridional winds at 850 hPa reveal reasonably the contributions of zonal wind shear and meridional wind convergence over eastern China in MOHC, MPI-M, CCCma, and NCAR. However, the northerly and easterly components tend to be more westward in CCCma, the southerly and westerly components are insufficient in BCC, and the zonal shear and meridional convergence are lacking in MRI.
- 5) Only CCCma can simulate the interdecadal enhancement of blocking at 500 hPa over Lake Baikal, which is similar to the result from the NCEP–NCAR reanalysis. Correlation analyses show that the summer precipitation over the YRV often corresponds with the Baikal and Okhotsk blockings in CCCma, which is similar to the relationship between the observed precipitation and H500 from the NCEP–NCAR reanalysis.
- 6) The spatial patterns and time evolutions of the SVD1 for winter T_s –winter H500, winter T_s –spring H500, winter T_s –summer H500, spring T_s –spring H500, spring T_s –summer H500, and summer T_s –summer H500 demonstrate that CCCma and the NCEP–NCAR reanalysis reasonably capture the summer blocking over the Baikal, which corresponds to the warming winter, spring, and summer T_s over most of the boreal mid- to high latitudes and the Arctic. That is, consistent warming over the Baikal and most other boreal mid- to high latitudes and the Arctic in winter and spring is very important for maintaining the summer positive blocking anomalies over the Baikal. We speculate that BCC and MPI-M cannot effectively simulate the enhancement of the Baikal blocking during 1990–2005 because their interdecadal variations of T_s over the mid- to high latitudes of Asia are often in opposite phase to the T_s variations in most other boreal mid- to high latitudes or their T_s enhancements are too small over the mid- to high latitudes of Asia during 1990–2005.

In summary, we demonstrate that CCCma can approximately simulate the increase of interdecadal precipitation over the YRV in 1990–2005 relative to 1960–75; the interdecadal warming of T_s over the boreal mid- to high latitudes and the Arctic in winter, spring, and summer; the relationships between the summer precipitation over the YRV and T_s ; zonal and meridional winds at 850 hPa; and the interdecadal enhancement of the Baikal blocking at 500 hPa and the correlation between winter, spring, summer T_s and H500 over the boreal mid- to high latitudes. However, the first leading modes of winter T_s –winter H500 and spring T_s –spring H500 do not reach the 95% confidence level for most simulations and the NCEP–NCAR reanalysis, so there are some uncertainties in the relationships between T_s and H500 in the various seasons. Overall, both CCCma and the NCEP–NCAR reanalysis capture the interdecadal enhancement of precipitation over the YRV and they both show some consistent relationships between the mid- to high-latitude and Arctic warming and circulation such as blockings and zonal wind shear and meridional wind convergence. On the other hand, other models that do

not capture the interdecadal enhancement of precipitation over the YRV all failed to capture some, if not all, the relationships discussed above. These provide strong evidence that Arctic/high-latitude warming plays an important role in the interdecadal variability of precipitation in eastern China. From our analyses of the various relationships, we postulate that the positive anomalies of Baikal blocking may be the bridge that links the warmer winter and spring T_s to the interdecadal increase of summer precipitation over the YRV.

This study highlights the importance of high-latitude processes so differences in model representations of sea ice and cold season processes could be important factors even for simulating monsoon variability in the low latitudes. We caution that interdecadal changes in rainfall can be related to other factors such as SST forcing, so whether the models that are analyzed can reproduce the relationships of interdecadal rainfall with other remote factors may also influence their abilities to produce the correct response to Arctic conditions. To clearly attribute model differences would require systematic model experiments to isolate the dominant factors that affect model skill. Future CMIP endeavors aligned with the goals to attribute model errors can significantly advance our understanding of uncertainty in model simulations and projections.

Acknowledgments. This study was supported by the Office of Science of the U.S. Department of Energy as part of the Regional and Global Climate Modeling Program, which supported the bilateral agreement between the U.S. Department of Energy and China Ministry of Science and Technology on regional climate research. Pacific Northwest National Laboratory is operated for the U.S. Department of Energy by Battelle Memorial Institute under Contract DE-AC05-76RLO1830. This work is also supported by the National Important Basic Research Program of China (2012CB957804) and by the Special Fund for Meteorological Scientific Research in the Public Interest of China Meteorological Administration (Grant GYHY201006022). The authors are grateful for the comments and suggestions provided by three anonymous reviewers that helped improve the paper.

REFERENCES

- Arai, M., and M. Kimoto, 2005: Relationship between springtime surface temperature and early summer blocking activity over Siberia. *J. Meteor. Soc. Japan*, **83**, 261–267.
- Bretherton, C. S., C. Smith, and J. M. Wallace, 1992: An intercomparison of methods for finding coupled patterns in climate data. *J. Climate*, **5**, 541–560.
- Budikova, D., 2009: Role of Arctic sea ice in global atmospheric circulation: A review. *Global Planet. Change*, **68**, 149–163.
- Chen, L.-T., and R.-G. Wu, 2000: Inter-annual and decadal variations of snow cover over Qinghai-Xizang Plateau and their relationship to summer monsoon rainfalls in China. *Adv. Atmos. Sci.*, **17**, 18–30.
- Chen, W., L.-H. Kang, and D. Wang, 2006: The coupling relationship between summer rainfall in China and global sea surface temperature (in Chinese). *Climatic Environ. Res.*, **11**, 259–269.
- Dagmar, B., 2009: Role of Arctic sea ice in global atmospheric circulation: A review. *Global Planet. Change*, **68**, 149–163.
- Ding, Y.-H., and G.-Q. Hu, 2003: A study on water vapor budget over China during the 1998 severe flood periods (in Chinese). *Acta Meteor. Sin.*, **61**, 129–145.
- , and J. C. L. Chan, 2005: The East Asian summer monsoon: An overview. *Meteor. Atmos. Phys.*, **89**, 117–142.
- , Z.-Y. Wang, and Y. Sun, 2008: Inter-decadal variation of the summer precipitation in East China and its association with decreasing Asian summer monsoon. Part I: Observed evidences. *Int. J. Climatol.*, **28**, 1139–1161.
- , Y. Sun, Z.-Y. Wang, Y.-X. Zhu, and Y.-F. Song, 2009: Inter-decadal variation of the summer precipitation in China and its association with decreasing Asian summer monsoon Part II: Possible causes. *Int. J. Climatol.*, **29**, 1926–1944.
- Duan, A.-M., F. Li, M.-R. Wang, and G.-X. Wu, 2011: Persistent weakening trend in the spring sensible heat source over the Tibetan Plateau and its impact on the Asian summer monsoon. *J. Climate*, **24**, 5671–5682.
- Gao, H., S. Yang, A. Kumar, Z.-Z. Hu, B.-H. Huang, Y.-Q. Li, and B. Jha, 2011: Variations of the East Asian mei-yu and simulation and prediction by the NCEP Climate Forecast System. *J. Climate*, **24**, 94–108.
- Hao, L.-S., J.-Z. Min, Y.-H. Ding, and J. Wang, 2010: Relationship between reduction of summer precipitation in north China and atmospheric circulation anomalies. *J. Water Resour. Prot.*, **2**, 569–576.
- Ho, C.-H., J.-H. Kim, K.-M. Lau, K.-M. Kim, D.-Y. Gong, and Y.-B. Lee, 2005: Interdecadal changes in heavy rainfall in China during the northern summer. *Terr. Atmos. Oceanic Sci.*, **16**, 1163–1176.
- Hu, Z.-Z., 1997: Interdecadal variability of summer climate over East Asia and its association with 500 hPa height and global sea surface temperature. *J. Geophys. Res.*, **102** (D16), 19 403–19 412.
- , S. Yang, and R. Wu, 2003: Long-term climate variations in China and global warming signals. *J. Geophys. Res.*, **108**, 4614, doi:10.1029/2003JD003651.
- Kalnay, E., and Coauthors, 1996: The NCEP/NCAR 40-Year Reanalysis Project. *Bull. Amer. Meteor. Soc.*, **77**, 437–471.
- Lau, K.-M., and H. Weng, 2001: Coherent modes of global SST and summer rainfall over China: An assessment of the regional impacts of the 1997–98 El Niño. *J. Climate*, **14**, 1294–1308.
- Lei, Y.-H., B. Hoskins, and J. Slingo, 2011: Exploring the interplay between natural decadal variation and anthropogenic climate change in summer rainfall over China. Part I: Observational evidence. *J. Climate*, **24**, 4584–4599.
- Li, F., and Y.-H. Ding, 2004: Statistical characteristic of atmospheric blocking in the Eurasia high-mid latitudes based on recent 30-year summers (in Chinese). *Acta Meteor. Sin.*, **62**, 347–354.
- Li, H.-M., A.-G. Dai, T.-J. Zhou, and J. Lu, 2010: Responses of East Asian summer monsoon to historical SST and atmospheric forcing during 1950–2000. *Climate Dyn.*, **34**, 501–514, doi:10.1007/s00382-008-0482-7.
- Li, Y.-F., and L. R. Leung, 2013: Potential impacts of the Arctic on interannual and interdecadal summer precipitation over China. *J. Climate*, **26**, 899–917.

- , S. P. Harrison, P. Zhao, and J.-H. Ju, 2009: Simulations of the impacts of dynamic vegetation on interannual and interdecadal variability of Asian summer monsoon with modern and mid-Holocene orbital forcings. *Global Planet. Change*, **66**, 235–252.
- Lin, H., and Z. Wu, 2011: Contribution of the autumn Tibetan Plateau snow cover to seasonal prediction of North American winter temperature. *J. Climate*, **24**, 2801–2813.
- Liu, Z., and M. Alexander, 2007: Atmospheric bridge, oceanic tunnel, and global climatic teleconnections. *Rev. Geophys.*, **45**, RG2005, doi:10.1029/2005RG000172.
- Ma, Y., W. Chen, S.-K. Fong, K.-C. Leong, and W.-K. Leong, 2012: Interannual and interdecadal variations of precipitation over East China during meiyu season and their relationships with the atmospheric circulation and SST (in Chinese). *Chin. J. Atmos. Sci.*, **36**, 397–410.
- Masson, D., and R. Knutti, 2011: Climate model genealogy. *Geophys. Res. Lett.*, **38**, L08703, doi:10.1029/2011GL046864.
- Mayer, M., and L. Haimberger, 2012: Poleward atmospheric energy transports and their variability as evaluated from ECMWF reanalysis data. *J. Climate*, **25**, 734–752.
- Meehl, G. A., J. M. Arblaster, J. M. Caron, H. Annamalai, M. Jochum, A. Chakraborty, and R. Murtugudde, 2012: Monsoon regimes and processes in CCSM4. Part I: The Asian–Australian monsoon. *J. Climate*, **25**, 2583–2608.
- Peng, S., and J. Fyfe, 1996: The coupled patterns between sea level pressure and sea surface temperature in the midlatitude North Atlantic. *J. Climate*, **9**, 1824–1839.
- Pu, B., S.-W. Wang, and J.-H. Zhu, 2008: An East Asian teleconnection mode in relation to summer precipitation in eastern China (in Chinese). *Adv. Climate Change Res.*, **4**, 17–20.
- Royer, J. F., S. Planton, and M. Déqué, 1990: A sensitivity experiment for the removal of Arctic sea ice with the French spectral general circulation model. *Climate Dyn.*, **5**, 1–17.
- Samel, A. N., and X.-Z. Liang, 2003: Understanding relationships between the 1998 Yangtze River flood and northeast Eurasian blocking. *Climate Res.*, **23**, 149–158.
- Taylor, K. E., R. J. Stouffer, and G. A. Meehl, 2012: An overview of CMIP5 and the experiment design. *Bull. Amer. Meteor. Soc.*, **93**, 485–498.
- Venegas, S. A., L. A. Mysak, and D. N. Straub, 1996: Evidence for interannual and interdecadal climate variability in the South Atlantic. *Geophys. Res. Lett.*, **23**, 2673–2676.
- Wallace, J. M., C. Smith, and C. S. Bretherton, 1992: Singular value decomposition of wintertime sea surface temperature and 500-mb height anomalies. *J. Climate*, **5**, 561–576.
- Wang, B., Q. Bao, B. Hoskins, G. Wu, and Y. Liu, 2008: Tibetan Plateau warming and precipitation change in East Asia. *Geophys. Res. Lett.*, **35**, L14702, doi:10.1029/2008GL034330.
- , J. Liu, J. Yang, T.-J. Zhou, and Z.-W. Wu, 2009: Distinct principal modes of early and late summer rainfall anomalies in East Asia. *J. Climate*, **22**, 3864–3875.
- Wang, C.-H., X.-Z. Liang, and A. N. Samel, 2011: AMIP GCM simulations of precipitation variability over the Yangtze River valley. *J. Climate*, **24**, 2116–2133.
- Wang, H.-J., 2001: The weakening of the Asian monsoon circulation after the end of 1970's. *Adv. Atmos. Sci.*, **18**, 376–386.
- , and Y. Zhang, 2010: Model projections of East Asian summer climate under the 'Free Arctic' scenario. *Atmos. Oceanic Sci. Lett.*, **3**, 176–180.
- Wang, L., W. Chen, W. Zhou, J. C. L. Chan, D. Barriopedro, and R. Huang, 2010: Effect of the climate shift around mid 1970s on the relationship between wintertime Ural blocking circulation and East Asian climate. *Int. J. Climatol.*, **30**, 153–158, doi:10.1002/joc.1876.
- Wang, Y., M. Qian, and W.-J. Zhu, 2006: Decadal characteristics of summer Eurasian blockings and its possible relation to precipitation over China. *J. Nanjing Inst. Meteor.*, **29**, 591–598.
- Weng, H., K.-M. Lau, and Y. Xue, 1999: Multi-scale summer rainfall variation over China and its long-term link to global sea surface temperature variation. *J. Meteor. Soc. Japan*, **77**, 845–857.
- Wu, B.-Y., R. Zhang, B. Wang, and R. D'Arrigo, 2009a: On the association between spring Arctic sea ice concentration and Chinese summer rainfall. *Geophys. Res. Lett.*, **36**, L09501, doi:10.1029/2009GL037299.
- , —, and —, 2009b: On the association between spring Arctic sea ice concentration and Chinese summer rainfall: A further study. *Adv. Atmos. Sci.*, **26**, 666–678.
- Wu, Z.-W., J.-P. Li, Z.-H. Jiang, and T.-T. Ma, 2012: Modulation of the Tibetan Plateau snow cover on the ENSO teleconnections: From the East Asian summer monsoon perspective. *J. Climate*, **25**, 2481–2489.
- Yang, F.-L., and K.-M. Lau, 2004: Trend and variation of China precipitation in spring and summer: Linkage to sea-surface temperatures. *Int. J. Climatol.*, **24**, 1625–1644.
- Yu, R.-C., B. Wang, and T.-J. Zhou, 2004: Tropospheric cooling and summer monsoon weakening trend over East Asia. *Geophys. Res. Lett.*, **31**, L22212, doi:10.1029/2004GL021270.
- Zeng, G., W.-C. Wang, and C.-M. Shen, 2012: Association of the rainy season precipitation with low-level meridional wind in the Yangtze River valley and north China. *J. Climate*, **25**, 792–799.
- Zhang, Y.-S., T. Li, and B. Wang, 2004: Decadal change of the spring snow depth over the Tibetan Plateau: The associated circulation and influence on the East Asian summer monsoon. *J. Climate*, **17**, 2780–2793.
- Zhao, H.-G., and X.-Z. Chen, 1990: The statistical analysis of atmospheric blocking in the Northern Hemisphere. *Meteorology*, **3**, 1–8.
- Zhao, P., S. Yang, and R.-C. Yu, 2010: Long-term changes in rainfall over eastern China and large-scale atmospheric circulation associated with recent global warming. *J. Climate*, **23**, 1544–1562.
- Zhou, T.-J., D.-Y. Gong, J. Li, and B. Li, 2009a: Detecting and understanding the multi-decadal variability of the East Asian summer monsoon—Recent progress and state of affairs. *Meteor. Z.*, **18**, 455–467.
- , and Coauthors, 2009b: The CLIVAR C20C project: Which components of the Asian–Australian monsoon circulation variations are forced and reproducible? *Climate Dyn.*, **33**, 1051–1068.